NASA TECHNICAL MEMORANDUM

NASA TM X-72809

NASA TM X-72809

LOW-SPEED WIND-TUNNEL TESTS OF A LARGE-SCALE BLENDED-ARROW ADVANCED SUPERSONIC TRANSPORT MODEL HAVING VARIABLE-CYCLE ENGINES AND VECTORING EXHAUST NOZZLES

By

Lysle P. Parlett and James P. Shivers

NATIONAL AERONAUTICS AND SPACE ADMINISTRATION
LANGLEY RESEARCH CENTER, HAMPTON, VIRGINIA 23665

1. Report No.	2. Government Accession No.	3. Recipient's Catalog No.
TM X-72809		

4. Title and Subtitle	5. Report Date
LOW-SPEED WIND-TUNNEL TESTS OF A LARGE-SCALE BLENDED-ARROW ADVANCED SUPERSONIC TRANSPORT HAVING VARIABLE-CYCLE ENGINES AND VECTORING EXHAUST NOZZLES	April 1976
	6. Performing Organization Code
7. Author(s)	8. Performing Organization Report No.
Lysle P. Parlett and James P. Shivers	
9. Performing Organization Name and Address	10. Work Unit No.
NASA Langley Research Center	743-04-12-02
Hampton, VA 23665	11. Contract or Grant No.
	13. Type of Report and Period Covered
12. Sponsoring Agency Name and Address	Technical Memorandum
National Aeronautics and Space Administration	14. Sponsoring Agency Code
Washington, DC 20546	

15. Supplementary Notes

16. Abstract

A low-speed wind-tunnel investigation has been conducted in the Langley full-scale tunnel to determine the performance and static stability and control characteristics of a large-scale model of a blended-arrow advanced supersonic transport configuration incorporating variable-cycle engines and vectoring exhaust nozzles. Configuration variables tested included: (1) engine mode (cruise or low-speed), (2) engine exit nozzle deflection, (3) leading-edge flap geometry, and (4) trailing-edge flap deflection. Test variables included values of C_μ from 0 to 0.38, values of angle of attack from -10° to 30°, values of angle of sideslip, from -5° to 5°, and values of Reynolds number, from 3.5 million to 6.8 million.

17. Key Words (Suggested by Author(s))	18. Distribution Statement
Blended-arrow supersonic transport Variable-cycle engines Vectored thrust Low-speed wind-tunnel tests	Unclassified - Unlimited

19. Security Classif. (of this report)	20. Security Classif. (of this page)	21. No. of Pages	22. Price*
Unclassified	Unclassified	5	$4.25

*For sale by the National Technical Information Service, Springfield, Virginia 22161

LOW-SPEED WIND-TUNNEL TESTS OF A LARGE-SCALE BLENDED-ARROW ADVANCED SUPERSONIC TRANSPORT MODEL HAVING VARIABLE-CYCLE ENGINES AND VECTORING EXHAUST NOZZLES

By Lysle P. Parlett and James P. Shivers

Langley Research Center

SUMMARY

A low-speed wind-tunnel investigation has been conducted in the Langley full-scale tunnel to determine the performance and static stability and control characteristics of a large-scale model of a blended-arrow advanced supersonic transport configuration incorporating variable-cycle engines and vectoring exhaust nozzles. Configuration variables tested included: (1) engine mode (cruise or low-speed), (2) engine exit nozzle deflection, (3) leading-edge flap geometry, and (4) trailing-edge flap deflection. Test variables included values of C_μ from 0 to 0.38, values of angle of attack from -10° to 30°, values of angle of sideslip, from -5° to 5°, and values of Reynolds number, from 3.5 million to 6.8 million.

The results of the investigation showed that, in the clean configuration, the model showed an unstable break in the pitching-moment curve (pitchup) at an angle of attack of about 5°. Deflection of inboard leading-edge flaps and the addition of a Krueger flap to the wing outer panels delayed the longitudinal instability to an angle of attack of about 20°. In either the cruise or low-speed engine mode, downward deflection of the engine exhaust nozzle produced significant increases in lift coefficient which were larger than the direct lift component of the thrust, indicating the presence of induced circulation lift. Nozzle deflection in conjunction with trailing-edge flap deflection produced an untrimmed lift coefficient of 0.87 at an angle of attack equal to the tail scrape angle ($\alpha = 10^\circ$). The model exhibited stable lateral-directional characteristics, and at high angles of attack showed large values of directional stability and positive effective dihedral.

INTRODUCTION

The present study is part of the overall NASA effort to provide the technology base for the development of advanced supersonic-cruise vehicles. One promising concept for an advanced arrow-wing supersonic transport designed for cruise near Mach 3 features a blended wing-body, vectoring exhaust nozzles, and variable-cycle engines. Preliminary tests of such a configuration (without the variable-cycle engine feature) have been previously reported in reference 1. Results of that investigation indicated a severe pitchup for the cruise configuration at low angles of attack and a maximum usable C_L of only about 0.5 for the landing configuration. Both of these undesirable characteristics were attributed to stall of the outer panels of the highly swept wing, and it was anticipated that improved characteristics could be obtained from reduced sweep of the outer wing panels and more efficient leading-edge devices.

The model used in the present investigation was produced by the foregoing outer-wing modifications to the model used in reference 1. In addition, engine exhaust doors representative of those required for variable-cycle operation were incorporated in the model. The objectives of the tests were to determine the improvements in low-speed performance provided by the wing modifications, and to determine the effectiveness of the vectoring nozzles in combination with the variable-cycle engine concept.

The tests were conducted in the Langley full-scale tunnel for a range of Reynolds numbers from 3.5×10^6 to 6.8×10^6 based on the mean aerodynamic chord. The tests were conducted for a range of angle of attack of -10° to 30° and for sideslip angles of $\pm 5^\circ$. The configuration variables included combinations of leading- and trailing-edge flap deflections; engine thrust, nozzle angle and variable-cycle mode; and lateral-directional control deflections.

SYMBOLS

The data are referred to the stability system of axes illustrated in figure 1. The origin of the axis system was located to correspond with the 38.7-percent location of the mean aerodynamic chord.

The dimensional quantities are given in the International System of Units (SI) and in U. S. Customary Units. Conversion factors for the two systems are given in reference 2.

b	wing span, 5.38 m (17.65 ft)
$\bar{c}$	mean aerodynamic chord, 4.37 m (14.35 ft)
C_D	drag coefficient, Drag/qS
C_L	lift coefficient, Lift/qS
C_ℓ	rolling-moment coefficient, Rolling Moment/qSb
C_{ℓ_β}	$\frac{\partial C_\ell}{\partial \beta}$, per degree
C_m	pitching-moment coefficient, Pitching Moment/qS$\bar{c}$
C_n	yawing-moment coefficient, Yawing Moment/qSb
C_{n_β}	$\frac{\partial C_n}{\partial \beta}$, per degree
C_Y	side force coefficient, side force/qS
C_{Y_β}	$\frac{\partial C_Y}{\partial \beta}$, per degree
C_μ	gross thrust coefficient, T/qS
l	distance from pitching moment reference to canard center of lift, m (ft)
q	free-stream dynamic pressure, N/m^2 (lbs/ft^2)
S	wing area, 16.54 m^2 (178 ft^2)
T	engine gross thrust, N (lbs)
α	angle of attack referred to wing reference line (fig. 2) deg
β	angle of sideslip, deg
δ	deflection of nozzle segment or aerodynamic surface, deg

δ_j deflection of engine exhaust jet, deg

δ_n leading-edge flap deflection, deg

δ_f trailing-edge flap deflection, deg

η static turning efficiency

Subscripts:

NOZ engine exhaust nozzle

1,2,3 (with δ_n symbol) wing leading-edge flap segments (1, nearest nose of model (see fig. 2))

1,2,3 (with δ_f symbol) wing trailing-edge flap segments (1, inboard, and 3, outboard (see fig. 2))

c canard

MODEL

The dimensional characteristics of the model are shown in figure 2 and listed in table 1; and a photograph of the model mounted for tests in the Langley full-scale tunnel is presented in figure 3. The general arrangement of the model, including principal dimensions, and the locations of the leading- and trailing-edge flaps are shown in figure 2(a). Details of the vectoring nozzle, and of the variable-cycle engine concept in the cruise and low-speed modes, are shown in 2(b) and 2(c), respectively. For both modes, thrust was supplied by eight compressed-air-driven engine simulators, each having a fan diameter of 5-1/2 inches, arranged in tandem banks of four each. In the cruise mode (figure 2(c)) the intake flow (the air passing through the fans) was common to both the forward and rearward banks of engines. In the low-speed mode, a diverter duct installed behind the forward bank of engines caused the airflow through the forward engines to be exhausted rearward over the top of the fuselage and vectoring nozzle. Inlet air for the rear engines was admitted through an opening in the bottom of the engine pod, and was exhausted through the vectoring nozzle, as in the cruise mode.

Details of the leading-edge and trailing-edge flaps are shown in figure 2(d). A leading-edge Krueger flap extended over only the outboard segment of the span, as shown in figure 2(d). Inboard of the Krueger flap, the wing leading edge could be drooped 60°, and in that position could be fitted with a bulbous leading-edge modification which increased the leading-edge radius. Except where specifically noted, in all cases in which the leading edge was drooped, the bulbous modification was also installed. The trailing-edge flaps were conventional unslotted surfaces, and the inboard panels could be deflected symmetrically or differentially.

The model was equipped with fixed twin vertical tails with full span rudders as shown in figure 2(a).

TESTS AND CORRECTIONS

Tests

Force tests of the model were made in the Langley full-scale tunnel at a free-stream dynamic pressure of 158 newtons/meter^2 (3.3 pounds/ft^2). The velocity corresponding to this dynamic pressure produced a Reynolds number of 4.8×10^6, based on the mean aerodynamic chord of the wing. For a limited number of power-off conditions, the effect of varying Reynolds number was investigated through a range of Reynolds numbers from 3.4×10^6 to 6.8×10^6. Angle of attack was varied from -10° to 30°, sideslip from +5° to -5°, and C_μ, in power-on runs, from 0 to 0.38. Configuration variables tested included: (1) engine mode (cruise or low-speed), (2) engine exit nozzle deflection, (3) leading-edge flap geometry, and (4) trailing-edge flap deflection.

The gross thrust of the engines was based on static (wind-off) thrust calibrations made for each individual bank of four, and for both banks (eight engines) operating simultaneously. For the wind-on tests, engine rotational speed was set at that value which produced the desired gross-thrust in the static condition. Previous tests of instrumented engines have shown that for relatively highly-loaded engines the gross thrust is insensitive to the low tunnel speeds of the present tests. The windmilling drag of the present engines was evaluated by measuring the difference in drag with the engines windmilling and with the engines being driven at a speed sufficient to produce an exhaust dynamic pressure equal to free-stream dynamic pressure, and was

applied as a correction to all power-off tests.

Wool tufts were attached to the wing upper surface to aid in the interpretation of the force test results.

Corrections

For all tests, corrections were applied for the drag and interference effects of the struts supporting the model, and for the drag of the exposed air-supply tubes. Angle of attack was corrected for tunnel airflow angularity, but no jet-boundary corrections were applied. Theory (reference 3) and tests had shown that such corrections would be negligible for the range of lift coefficients of the present tests.

PRESENTATION OF DATA

Type of data:	Figure Number
Longitudinal:	
Effect of Reynolds number	4
Effect of wing planform	5
Effect of leading-edge devices	6
Tuft studies	7, 8
Effect of trailing-edge flaps (power-off)	9
Effect of combined leading- and trailing-edge devices (power-off)	10
Effect of combined leading- and trailing-edge devices (power-on)	11
Individual contributions of flap and nozzle	12
Static turning and efficiency	13
Effectiveness of nozzle in producing added circulation lift	14
Comparison of several methods of achieving pitch trim	15
Effect of deflecting inboard segments of trailing-edge flap	16
Effect of deflecting engine exhaust nozzle	17
Comparison of longitudinal control effectiveness produced by deflection of various trailing-edge control devices	18

RESULTS AND DISCUSSION

Longitudinal Characteristics

Effect of Reynolds number.- Presented in figure 4 are data showing the effects of variations in Reynolds number on the longitudinal characteristics of the model (power-off). The data of figure 4 show that an increase in Reynolds number from 3.5×10^6 to 6.8×10^6 (produced by varying tunnel free-stream velocity from 22 to 44 knots) produced no significant changes in any of the longitudinal characteristics. In view of the lack of an appreciable effect of Reynolds number for the present configuration, data were obtained at a Reynolds number of 4.8×10^6 for most of the tests.

Effect of planform.- Figure 5 compares data from the present tests with results from reference 1 for the unmodified wing. Pitching-moment data from reference 1 have been transferred to the moment reference of the present model (0.387 $\bar{c}$) for the comparison. As was previously noted, the planform of the present model differs from that of the model of reference 1 in having less sweep in the outboard panels of the wing, more span, and more wing area. Figure 5 shows that the wing modifications increased the static longitudinal stability at low to moderate angles of attack and increased the angle of attack at which longitudinal instability (pitchup) occurred. The wing modifications also increased the lift-curve slope and resulted in a relatively small increase in the maximum value of L/D.

The effects of wing leading-edge devices are shown in figure 6. The contribution of the increased leading-edge radius was negligible for the conditions investigated, possibly because the bulbous leading edge was tested in combination with a relatively high leading-edge droop angle. The high droop angle alone was probably sufficient for suppressing the leading-edge vortex formation and the associated longitudinal instability (pitch-up) to a higher angle of attack. It is possible that the bulbous leading edge would have been effective for suppressing the leading-edge vortex formation if smaller leading-edge droop angles had been used in the tests. The Krueger flap, by itself, produced considerable improvements in the longitudinal characteristics; and the combination of leading-edge droop and Krueger flap produced a significant increase in longitudinal stability in the angle-of-attack range from 5° to 20° and, as a result, a delay in the value of α associated with pitch-up. Lift increments produced by leading-edge treatment were modest and were noticeable only at high angles of attack. The data also show that the combination of leading-edge droop angle and Krueger flap, which was beneficial to the longitudinal stability, also produced a slight increase in the maximum lift-drag ratio.

Tuft studies.- Figures 7 and 8 present photographs of tufts on the upper surface of the model in the clean configuration and with full leading-edge treatment, respectively. One characteristic of the flow for the clean configuration (figure 7) was that spanwise flow occurred over the wing center section and outboard panels. Such flow is typical of highly-swept configurations and this tendency was observed to increase in intensity as the angle of attack increased. In the present case, the flow pattern was apparently caused by the action of two vortices; one originating at the wing-fuselage juncture at the nose of the model, and the other at the sweep break in the wing leading edge. The spanwise component of the flow is first apparent near the wing trailing edge at an angle of attack of about -2.2°. At angles of attack above 1.6°, the spanwise flow is much more pronounced over the wing panels outboard of the leading-edge break than over the inboard sections. Constraints imposed by the vertical tails may account for these differences in spanwise flow intensity over the inboard and outboard wing sections. At an angle of attack of 5.6° the tufts at the wing tips indicate the onset of flow separation and this problem is apparently responsible for the destabilizing trends shown in the data at that angle of attack in figure 6.

Figure 8 shows that with the full leading-edge treatment applied (drooped leading edge and increased leading-edge radius inboard of the wing break, and Krueger flaps on the outer wing panels), the flow over the inboard wing panels was essentially the same as that for the clean configuration, indicating that the drooped leading edge and the increased radius had little effect on the basic flow pattern. The Krueger flap, however, apparently exerted a powerful influence on the flow outboard of the wing break in that the development of spanwise flow was delayed and did not become prominent until α was increased to 13.7°. Apparently the preservation of chordwise flow over the outboard areas produced a change in lift distribution which was mainly responsible for both the improvement in static stability and lift characteristics shown in figure 6.

Effect of trailing-edge flaps (power-off).- The effects of deflecting the trailing-edge flaps (in conjunction with full leading-edge treatment) are shown in figure 9. The data of figure 9 is for the model with the entire trailing edge deflected and, as expected, the data show that positive flap deflections produced sizable lift increments and large nose-down pitching moments. Because these effects are about the same for flap deflections of 20° and 30°, flow separation on the 30° flap configuration is suspected. The maximum value of L/D for the 20° flap configuration is as high as that for the undeflected case, suggesting that the increased circulation associated with the higher lift is also probably producing an increase in leading-edge suction on the Krueger flap. Deflecting the flap had little or no effect on the maximum value of L/D until the deflection reached 30°, where some separation may have developed. Comparison of data for the cruise engine mode (figure 9(a)) and for the low-speed engine mode (figure 9(b)) shows that in the power-off condition the engine configuration did not influence the aerodynamic characteristics of the model.

Figure 10 shows that with full leading-edge treatment, the present model exhibits a steeper lift-curve slope and much more longitudinal stability than the model of reference 1. The data also show that flap deflection produced considerably more lift and pitching moment for the present model. The more favorable characteristics of the present model are attributable to the lesser sweep of the outboard wing panels and to the increased effectiveness of the Krueger flap in delaying flow separation compared to that of the plain drooped leading-edge flap of the model of reference 1. As a result of the increased

longitudinal stability a much more aft center-of-gravity location could be tolerated for the present model and still maintain static longitudinal stability. This point will be discussed in more detail in a subsequent section of the present paper.

Effect of leading- and trailing-edge flaps (power-on).- Deflection of the engine exhaust nozzle in conjunction with leading- and trailing-edge flap deflection produced the results shown in figure 11. At a C_μ of 0.38 and in either engine mode, the combination of deflected nozzle and trailing-edge flaps produced high lift coefficients, large diving moments, and increased the stall angle of attack with little or no change in the longitudinal stability characteristics. Comparison of figures 9(a) and 11(a) shows that vectoring the exhaust nozzle (with flaps already down) gave an increase in C_L at the tail scrape angle from 0.65 to 0.89, or permitted the C_L of 0.65 to be obtained at an α of 4° rather than of 10°. Note that, in terms of practical application, these are untrimmed conditions; and that some means of achieving trim without penalizing lift must be employed to realize the lift benefits shown in figure 11. A method for achieving pitch trim will be discussed in the following section. Note also that the thrust loss accompanying nozzle deflection might be prohibitively high for the 30° nozzle deflection, and that the 30° flap deflection may be inferior to the 20° deflection because of the possibility of flow separation at the higher flap angles. The data does show, however, the possibility for increasing take-off C_L and for reducing take-off α.

Figure 12 is a summary plot of the longitudinal data presented to show the individual contributions to the longitudinal characteristics. At an α of 10° and a C_μ of 0.38, the changes in lift and pitching moment produced by vectored thrust are approximately equal to those produced by 30° deflection of the entire trailing-edge flap. Vectoring the thrust in either the cruise or low-speed engine modes (compare figure 12(a) and 12(b)) produced pitching moments and lift characteristics which were generally similar, but the low-speed engine mode showed higher drag characteristics than the cruise engine mode.

Figure 13 presents the static turning characteristics of the model in the low-speed engine configuration with the upper part of the exhaust nozzle

deflected 30°. The data show that 14° of turning were obtained at an efficiency of 78 percent. In figure 14 the sum of the lift component of the vectored thrust ($C_\mu \sin(\delta_j + \alpha)\eta$) and the power-off lift ($C_{L,0}$) produce, at a C_μ of 0.38, a C_L of 0.63. The measured C_L was 0.70, indicating the presence of added circulation lift ($C_{L,\Gamma}$) of 0.07. The data of figure 12 show that the combination of thrust vectoring and flap deflection increased C_L from 0.4 to 0.87 at the tail scrape angle of attack ($\alpha = 10°$). As pointed out in reference 4, the increased lift permits operation at lower angles of attack during the take-off and landing phases of flight. Lower angles of attack would allow reduced landing gear length and would eliminate the requirement for deflection of the fuselage nose. Elimination of these features could result in a significant weight reduction. Also, the wing area may be reduced, which would result in an additional weight savings, and would permit a better match in engine and airframe components for increased operational efficiency in cruise.

Pitch trim considerations.- One of the problems associated with the use of vectored thrust and sizable flap deflections for high lift in the accompanying large diving moments, as shown in the data of figure 12. In the investigation of reference 4 it was shown that the use of an all-movable, retractable canard provided, at no cost to lift, the moments necessary to provide pitch trim for arrow-wing supersonic transport configurations employing powered lift. On the basis of those results, a brief study was made to examine the use of the following arrangements for providing pitch trim:

1. Fixed canard
2. Free-floating canard
3. Canard driven in proportion to α.

The effectiveness of the canard configurations for providing trim and stability was examined for conditions corresponding to those obtained for the model with a trailing-edge flap deflection of 30° and a value of thrust coefficient of 0.38 (see figure 12). The analysis was conducted using the equations presented in reference 5 and required the configuration to provide longitudinal trim, a three-percent static margin, and a trimmed lift coefficient of 0.8. For analysis purpose, the canard was assumed to have a lift-curve slope of 0.06 per degree, non-dimensional tail length (l/c) of 1.2, and ϵ downwash

factor $(1-d\varepsilon/d\alpha)$ of 1.0. For the geared canard, a lift-curve slope of -0.06 per degree was assumed, corresponding to a canard gear ratio $\frac{\Delta i_c}{\Delta\alpha} = -2.0$.

A range of canard area ratios S_c/S from 0 to 0.10 was evaluated; and the center of gravity position was allowed to vary so as to maintain a constant level of static margin as the canard area varied. The results of the study are presented in figure 15 in terms of the canard lift coefficient, $C_{L,c}$ required for the range of S_c/S.

The data of figure 15(a) show that for a maximum canard lift coefficient of 2.5 (a value well within the capability of a good high lift system), a fixed canard surface having an area of about 4.5 percent of the wing area would provide pitch trim and a three-percent static margin. For the free-floating canard (or for a canard surface mechanically driven such that its incidence angle does not change as the airplane angle of attack changes), pitch trim could be achieved for a value of S_c/S of only about 0.032 and a canard lift coefficient of 2.5. For the canard arrangement which is mechanically driven such that its incidence angle is reduced as the airplane angle of attack is increased, the canard size could be reduced to a value of S_c/S of about 0.023 at a lift coefficient of 2.5.

Presented in figure 15(b) is the variation of center of gravity location as a function of S_c/S to maintain a static margin of three percent for the trim devices discussed in figure 15(a). The data show that the center-of gravity range for achieving pitch trim and stability for the three canard configurations investigated is relatively far aft.

It is of interest to note that the free-floating canard and geared canard arrangements allow a more aft center-of-gravity location than does the fixed canard configuration in satisfying the requirements for pitch trim and static stability. This result is significant in that it may permit the use of an aft center of gravity location in low speed flight which is consistent with that for supersonic cruise flight, thus minimizing the usual balance problem between the two speed ranges.

Control effectiveness.- Basic longitudinal data for the model with the inboard flap segments and the engine exhaust nozzle deflected for longitudinal

control are presented in figures 16 and 17, respectively. To provide direct comparisons, selected data from these plots, from previous plots, and from reference 1 are presented as a summary plot in figure 18. The data of figure 18 show that combinations of trailing-edge deflection and nozzle deflection can produce pitching-moment coefficients of about 0.15 through the range of operational angles of attack. Apparently a lift carry-over effect contributes to the pitching moment, as the moments measured for the combination are noticeably greater than the sum of those measured for each component. As was mentioned in the discussion of figure 10, the control moments produced by the trailing-edge flaps of the present model are appreciably larger than those produced by the model of reference 1.

Performance comparison.- A comparison of the performance of the two engine modes (cruise and low-speed) is provided by figure 19 in terms of the thrust-weight ratios required at various lift coefficients for a 3° climb angle and a 3° descent angle. The results shown are based on flap-down data from figure 11, and the data show that in either the climb or descent condition, somewhat less thrust is required in the cruise mode than in the low-speed mode - approximately 10 percent less at an angle of attack equal to the tail scrape angle (10°).

Lateral-Directional Characteristics

The lateral-directional characteristics of the model of the present investigation together with similar data for the model of reference 1 are presented in figure 20 in terms of the side-force derivative C_{Y_β}, directional stability derivative C_{n_β}, and effective dihedral derivative C_{ℓ_β}. The magnitude of the derivatives were determined from values of the respective coefficients at values of β of $\pm 5°$. The data of figure 20(a) show that the models were directionally stable at low angles of attack, and the level of directional stability increased markedly as the angle of attack was increased such that the configurations were extremely stable at high angles of attack. It should be noted that the high value of directional stability at high angles of attack is accompanied by large positive values of C_{Y_β}. An analysis of the relative signs of the two derivatives indicates that the aerodynamic stabilizing moment was produced forward of the center of gravity position. Past investigations have shown that the foregoing characteristics may be related to the

action of vortices shed from the nose of the model at high angles of attack (see ref. 1). The level of directional stability for the model of reference 1 was much higher than that for the present model over the test angle of attack range. This difference in C_{n_β} for the two models is not clearly understood but may be related to the differences in sweep of the outboard panels. Another factor which may be important in this comparison is that the outer panels of the present model were equipped with a large Krueger flap whereas for the model of reference 1, a plain drooped flap was used.

The data of figure 20(a) show good agreement in C_{ℓ_β} for the two models at low angles of attack, and that C_{ℓ_β} increased linearly with α up to $\alpha = 12^\circ$ for the model of reference 1 and up to about 20° for the present model. Above these angles of attack, the value of C_{ℓ_β} decreased rapidly for each model. The marked reduction in C_{ℓ_β} is apparently related to the stall of the advancing wing panels. A comparison of figures 20(a) and 20(b) shows that the lateral-directional characteristics are not sensitive to changes in engine configuration or to engine thrust levels.

Lateral-Directional Control Characteristics

The main objective of the present investigation was to investigate the longitudinal characteristics of the model. For this reason, no provision was made for differential deflection of the outboard trailing-edge surfaces. It was possible, however, to deflect the inboard trailing-edge surfaces differentially. Tests were therefore conducted to evaluate the use of inboard surfaces for roll control and the results are presented in figure 21 for the model in the low-speed engine configuration. Data showing rudder effectiveness are presented in figure 22.

The data of figure 21 show that deflection of $\pm 30^\circ$ of the inboard surfaces produced an increment of C_ℓ of only about 0.02. Some increase in control effectiveness is noted with increasing thrust, indicating that some flow was probably induced over the flaps as thrust was increased. It should be noted, however, that the magnitude of roll control obtained in the present tests is relatively small for satisfactory operational conditions in the landing and take-off modes where crosswinds produced large roll control requirements

(see reference 1). It is possible that differential deflections of full-span trailing-edge flaps could produce substantial increase in roll control of the present model.

One significant point to be noted about the data of figure 21 is that the inboard surfaces produced relatively large adverse yawing moments. In fact, a comparison of the data of figures 21 and the lateral-directional data with rudders deflected (figure 22) shows that the adverse yawing moments produced by differential deflection of the inboard elevon surfaces was about equal to the favorable yawing moments produced by 30° deflection of the rudders. Rudder effectiveness is noted to decrease with increasing angle of attack and the rudders become ineffective for directional control at an angle of attack of about 20°.

CONCLUDING REMARKS

Force tests of a large-scale model of an advanced blended-arrow supersonic transport model having variable-cycle engines and vectoring exhaust nozzles show the following results:

1. In the clean configuration, the model exhibited an unstable break in the pitching-moment curve at an angle of attack of about 5°. Deflection of inboard leading-edge flaps and the addition of a Krueger flap to the wing outer panels delayed longitudinal instability to an angle of attack of about 20°.

2. In either the cruise or low-speed variable-cycle engine mode, downward deflection of the engine exhaust nozzle produced significant increases in lift coefficient. These increases were larger than the direct lift component of the thrust, indicating the presence of induced circulation lift. Nozzle deflection in conjunction with trailing-edge flap deflection produced an untrimmed lift coefficient of 0.87 at an angle of attack equal to the tail scrape angle ($\alpha = 10°$).

3. The model exhibited stable lateral-directional characteristics, and at high angles of attack large values of directional stability and positive effective dihedral were obtained.

REFERENCES

1. McLemore, H. Clyde; and Parlett, Lysle P.: Low-Speed Wind-Tunnel Tests of A 1/10-Scale Model of a Blended-Arrow Advanced Supersonic Transport. NASA TM X-72671, 1975.

2. Mechtly, E. A.: The International System of Units - Physical Constants and Conversion Factors (Second Revision). NASA SP-7012, 1975.

3. Heyson, Harry H.: Use of Superposition in Digital Computers to Obtain Wind-Tunnel Interference Factors for Arbitrary Configuration, With Particular Reference to V/STOL Models. NASA TR R-302, 1969.

4. Shivers, James P.; McLemore, H. Clyde; and Coe, Paul L., Jr.: Low-Speed Wind-Tunnel Investigation of a Large-Scale Advanced Arrow-Wing Supersonic Transport Configuration with Engines Mounted Above the Wing for Upper-Surface Blowing. NASA TM X-72761, 1975.

5. Johnson, Joseph L.: Wind-Tunnel Investigation of the Static Longitudinal Stability and Trim Characteristics of a Sweptback-Wing Jet-Transport Model Equipped With An External-Flow Jet Augmented Flap. NACA TN-4177, 1958.

National Aeronautics and Space Administration
Langley Research Center, Hampton, Va.
December 12, 1975

Table I

Dimensions of Model

Wing:		
Area, m^2 (ft^2)	16.54	(178)
Span, m (ft)	5.38	(17.65)
Aspect ratio		1.75
Length of mean aerodynamic chord, m (ft)	4.37	(14.35)
Location of quarter-chord of mean aerodynamic chord, referenced to nose of model, m (ft)	4.73	(15.52)
Spanwise station of mean aerodynamic chord, m (ft)	0.86	(2.83)
Tip chord, m (ft)	0.78	(2.55)
Moment Reference:		
Longitudinal location, referenced to nose of model, m (ft)	5.33	(17.48)
Vertical location, referenced to waterline of fuselage reference plane, m (ft)	-0.70	(-2.31)
Vertical Tail:		
Area (each tail), m^2, (ft^2)	0.56	(6.07)
Span, m (ft)	0.54	(1.76)
Length of mean aerodynamic chord, m (ft)	1.20	(3.95)
Longitudinal location of 0.25 c, referenced to nose of model, m (ft)	6.85	(22.46)
Aspect ratio		0.51
Root chord, m (ft)	1.76	(5.76)
Tip chord, m (ft)	0.34	(1.10)
Sweep Angles:		
Leading edge, deg		73.6
Trailing edge, deg		23.8
Control-Surface Dimensions:		
Rudder:		
Span, m (ft)	0.60	(1.96)
Chord, upper end, m (ft)	0.17	(0.55)
Chord, lower end, m (ft)	0.23	(0.76)
Sweep of hinge line, deg		29.8

Table I.- Concluded.

Segment of trailing-edge flap inboard of vertical tails:		
Span, m (ft)	0.78	(2.55)
Chord, outboard, m (ft)	0.40	(1.32)
Chord, inboard, m (ft)	0.51	(1.68)
Sweep of hinge line, deg		28.2
Segment of trailing-edge flap outboard of vertical tails:		
Span, m (ft)	1.55	(5.07)
Chord, outboard, m (ft)	0.27	(0.89)
Chord, inboard, m (ft)	0.40	(1.32)
Sweep of hinge line, deg		37

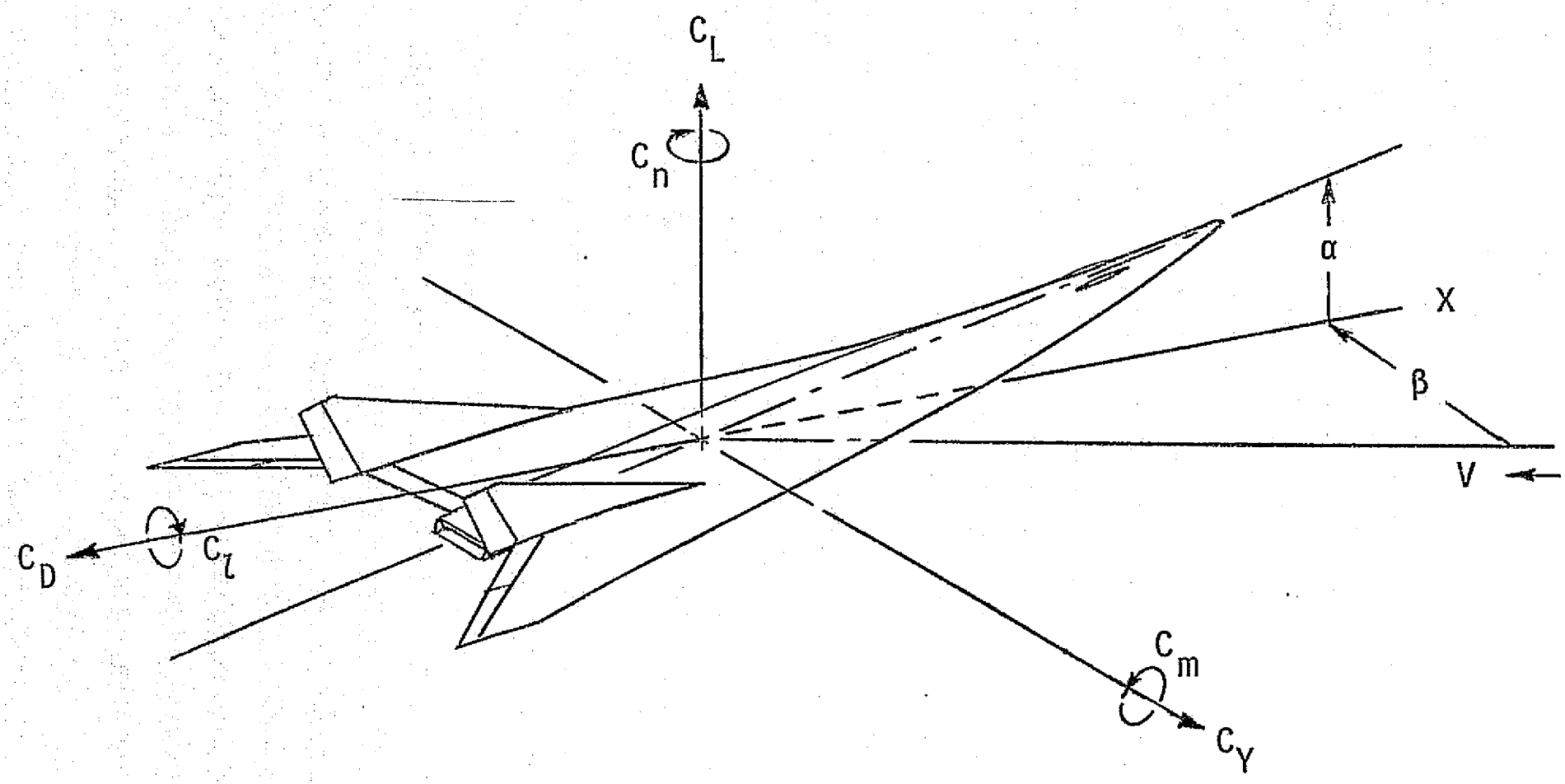

Figure 1. - System of stability axes and positive sense of angles, forces, and moments.

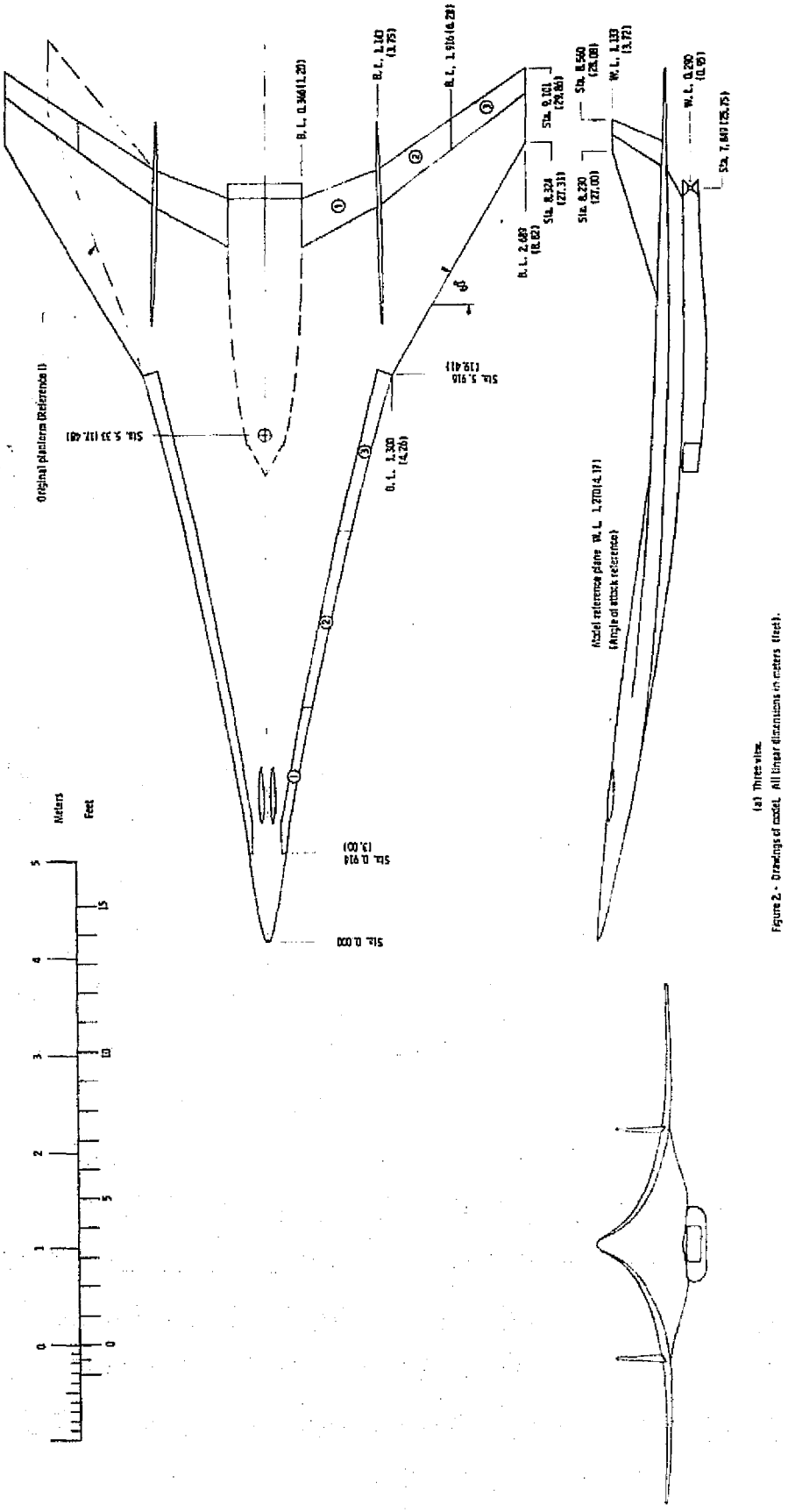

(a) Three view.

Figure 2.- Drawings of model. All linear dimensions in meters (feet).

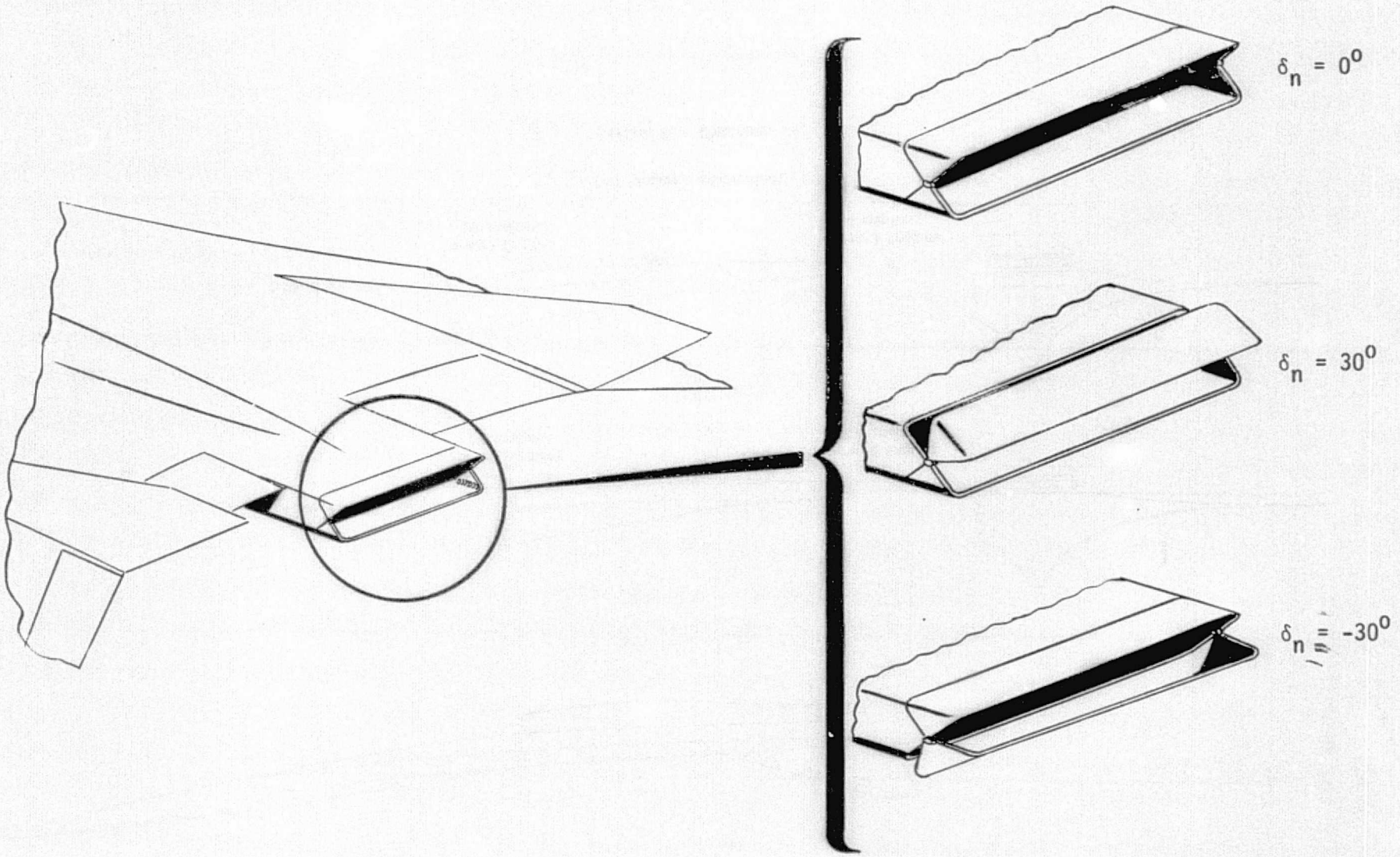

(b) Engine exit nozzle details.

Figure 2. - Continued.

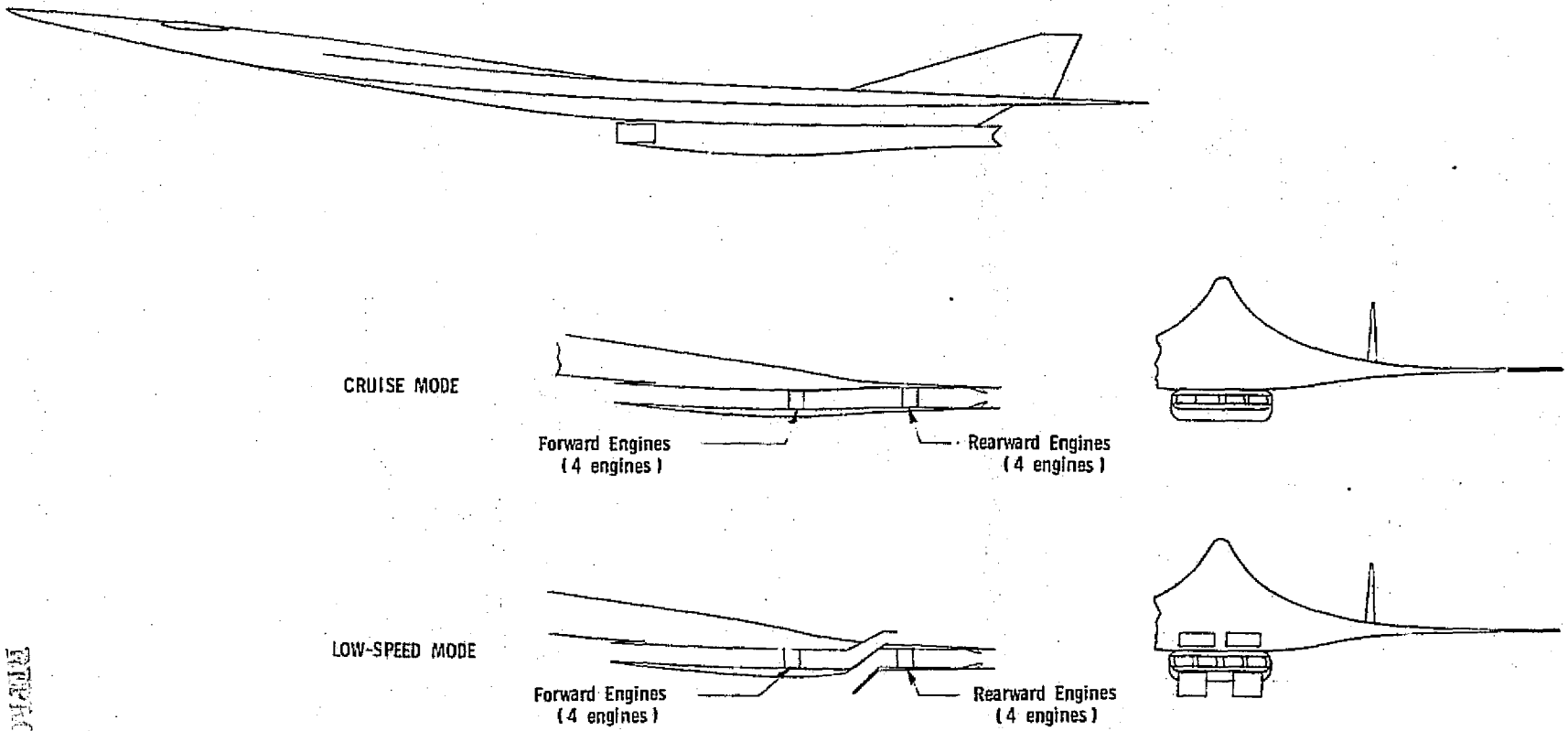

(c) Engine configurations.

Figure 2.- Continued.

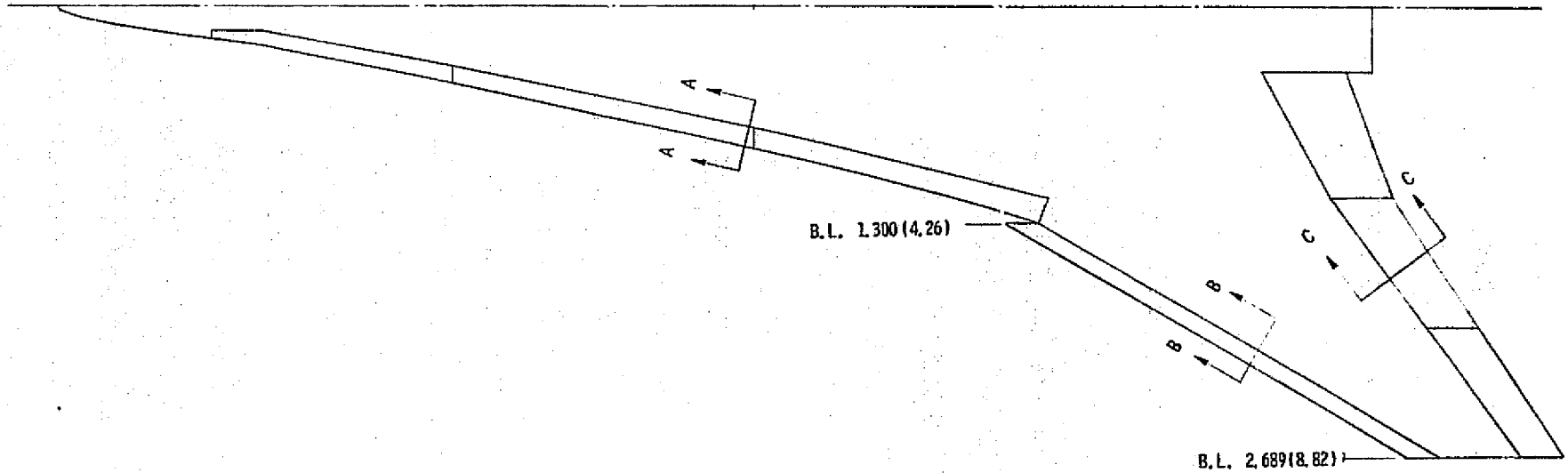

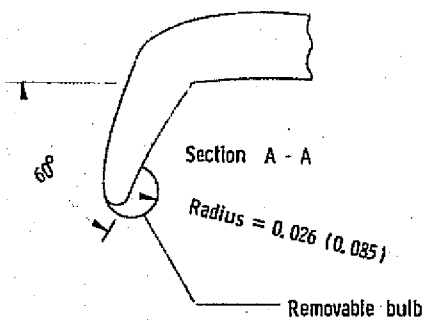

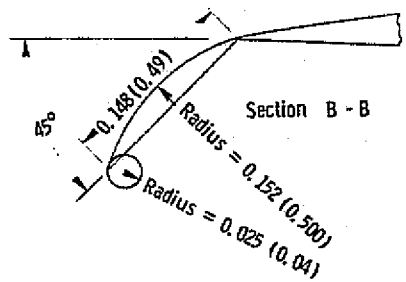

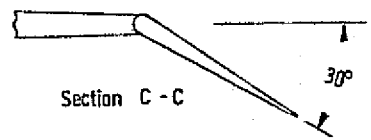

(d) Flap details.

Figure 2. - Concluded.

Figure 3.- Three-quarter rear view of model mounted for tests in the Langley full-scale tunnel.

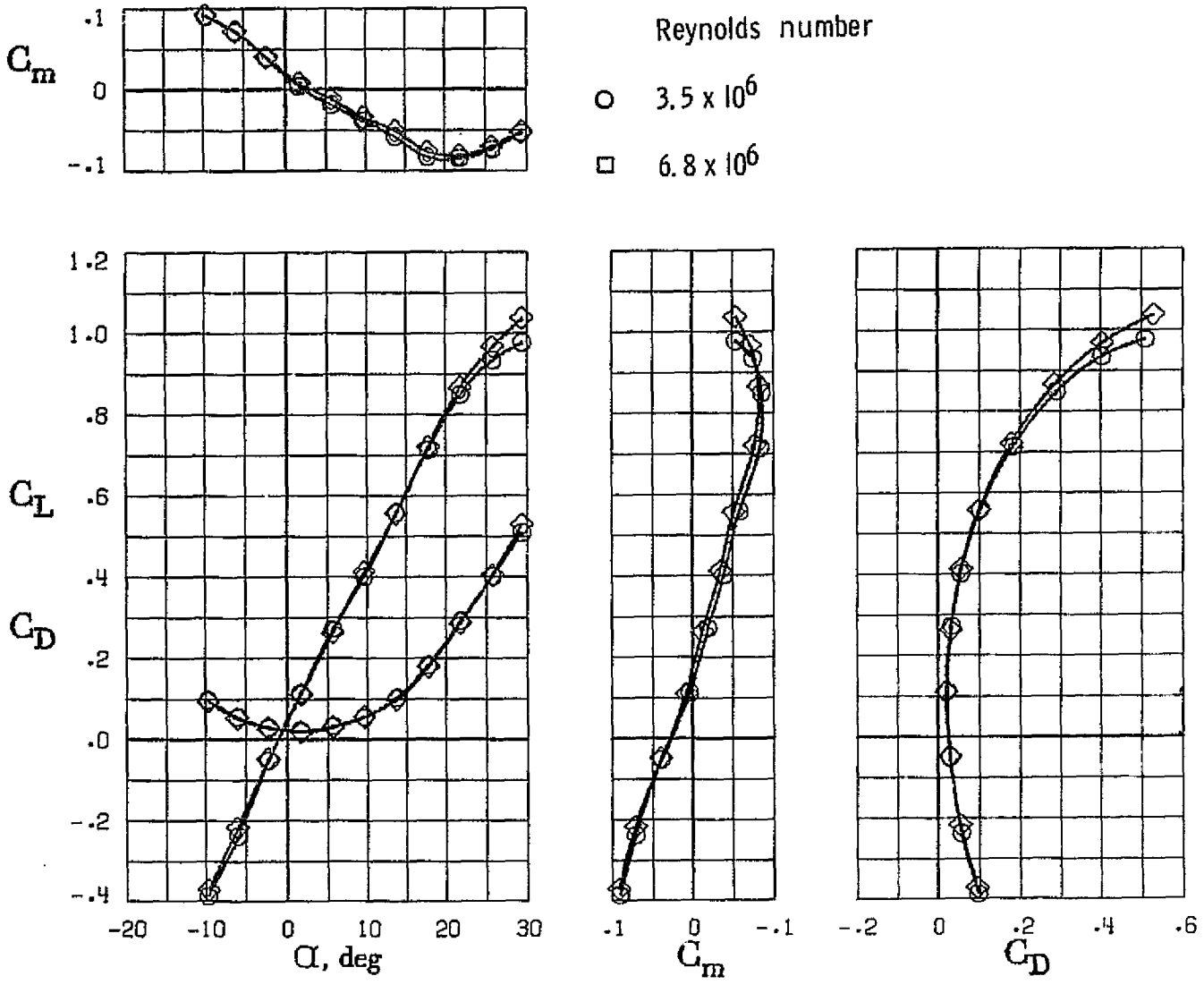

Figure 4. - Effect of Reynolds number. $\delta_{n,\ 1,2,3} = 60°$. Krueger on. Cruise engine mode. $\delta_f = 0°$. $\delta_{NOZ} = 0$. $C_\mu = C$.

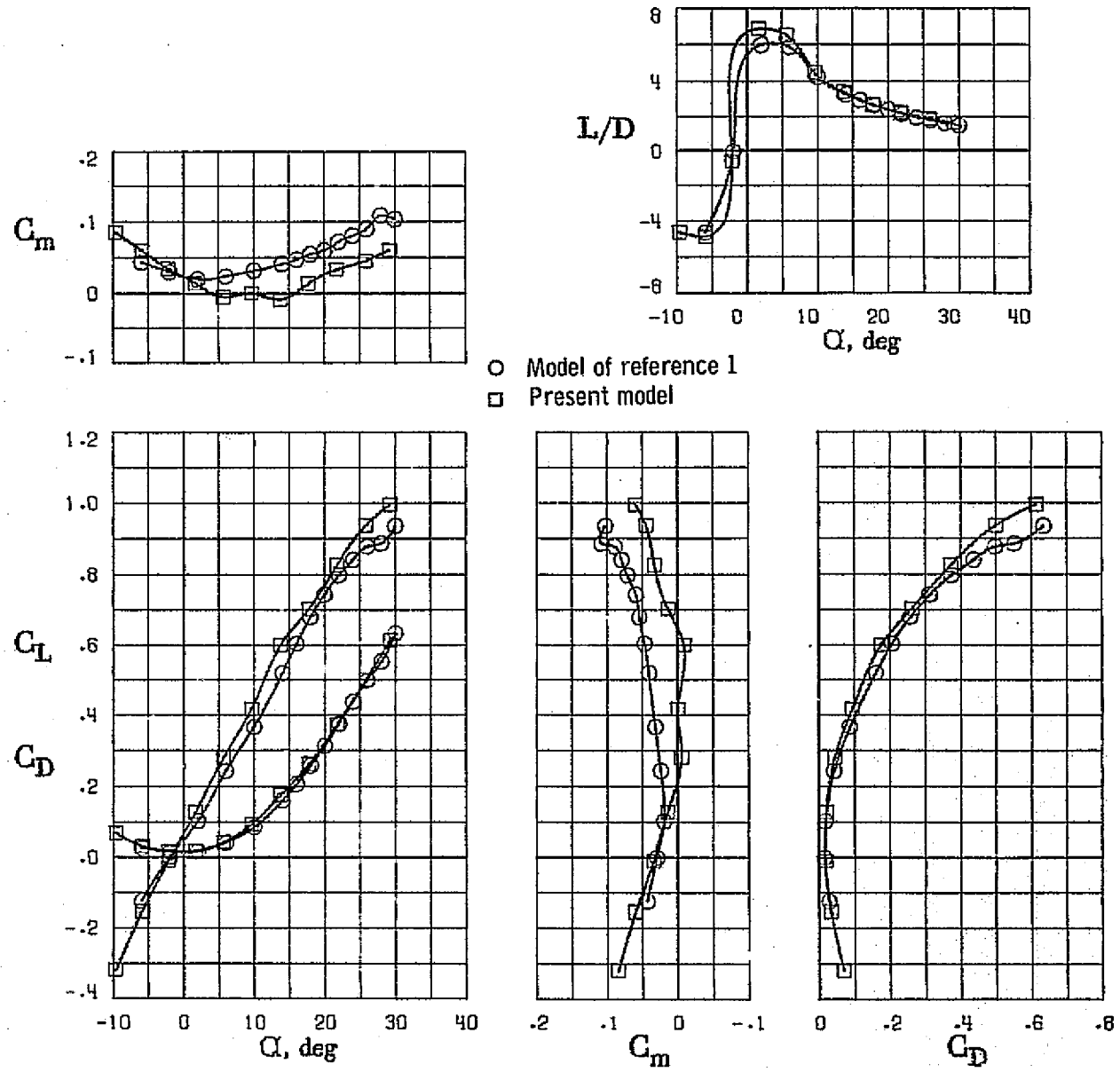

Figure 5. - Effect of wing planform on longitudinal characteristics. $\delta_n = 0°$, $\delta_f = 0°$. $\delta_{NOZ} = 0°$ $C_\mu = 0$.

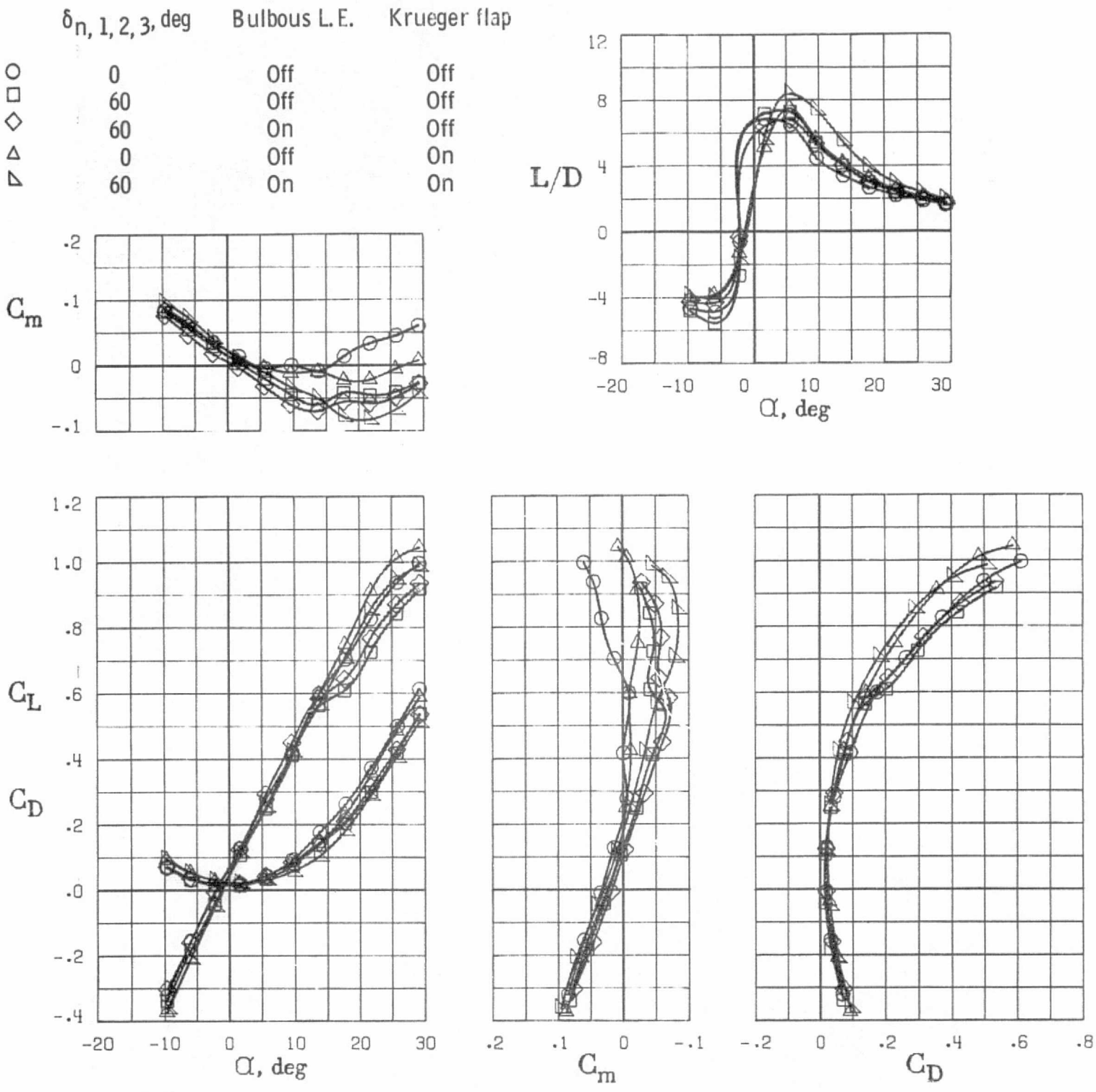

Figure 6. - Effect of various leading-edge devices on longitudinal characteristics. $\delta_{NOZ} = 0$. $C_\mu = 0$. Cruise engine mode. $\delta_f = 0$.

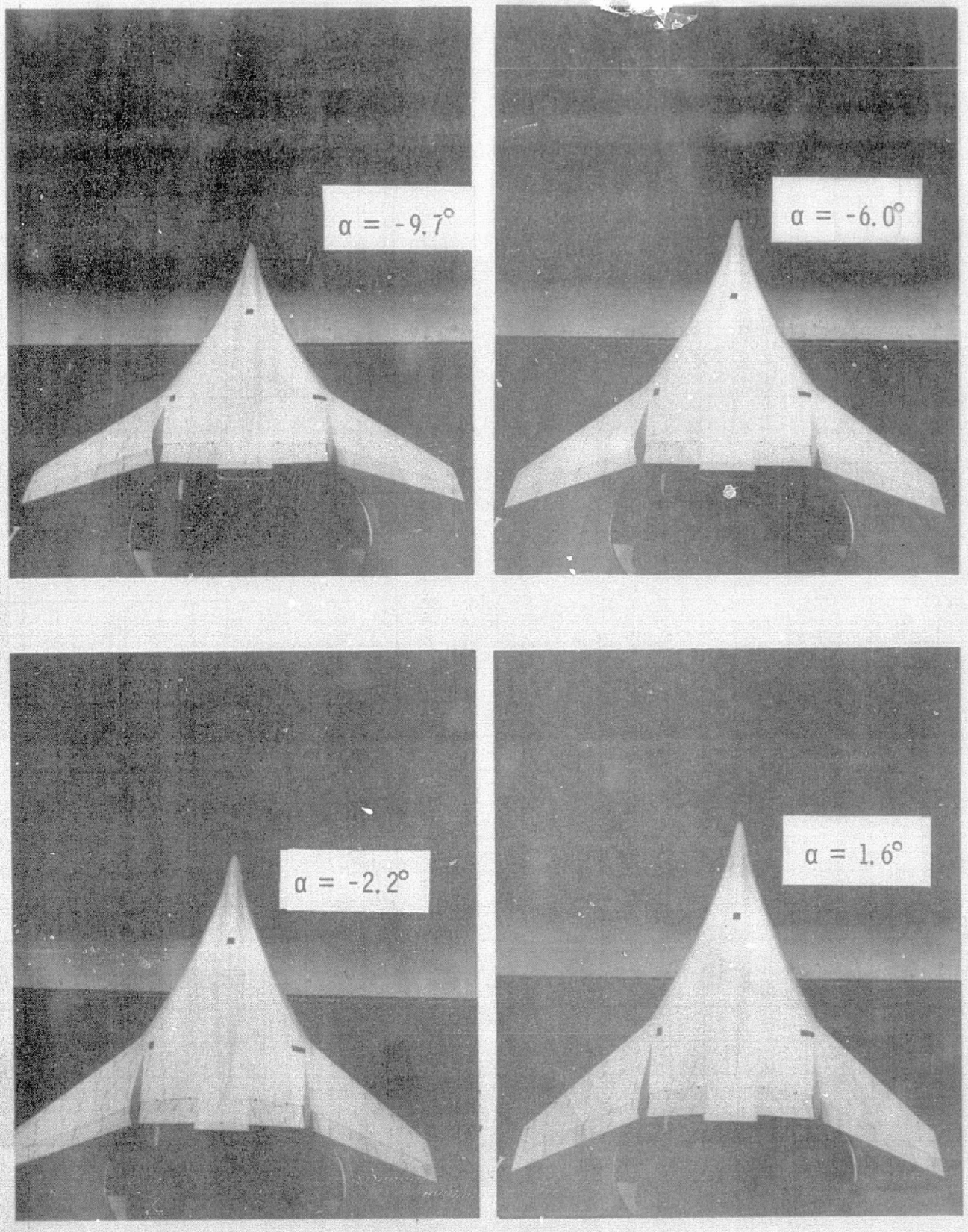

Figure 7. - Tuft photographs. $\delta_n = 0°$, $\delta_f = 0°$, $C_\mu = 0$.

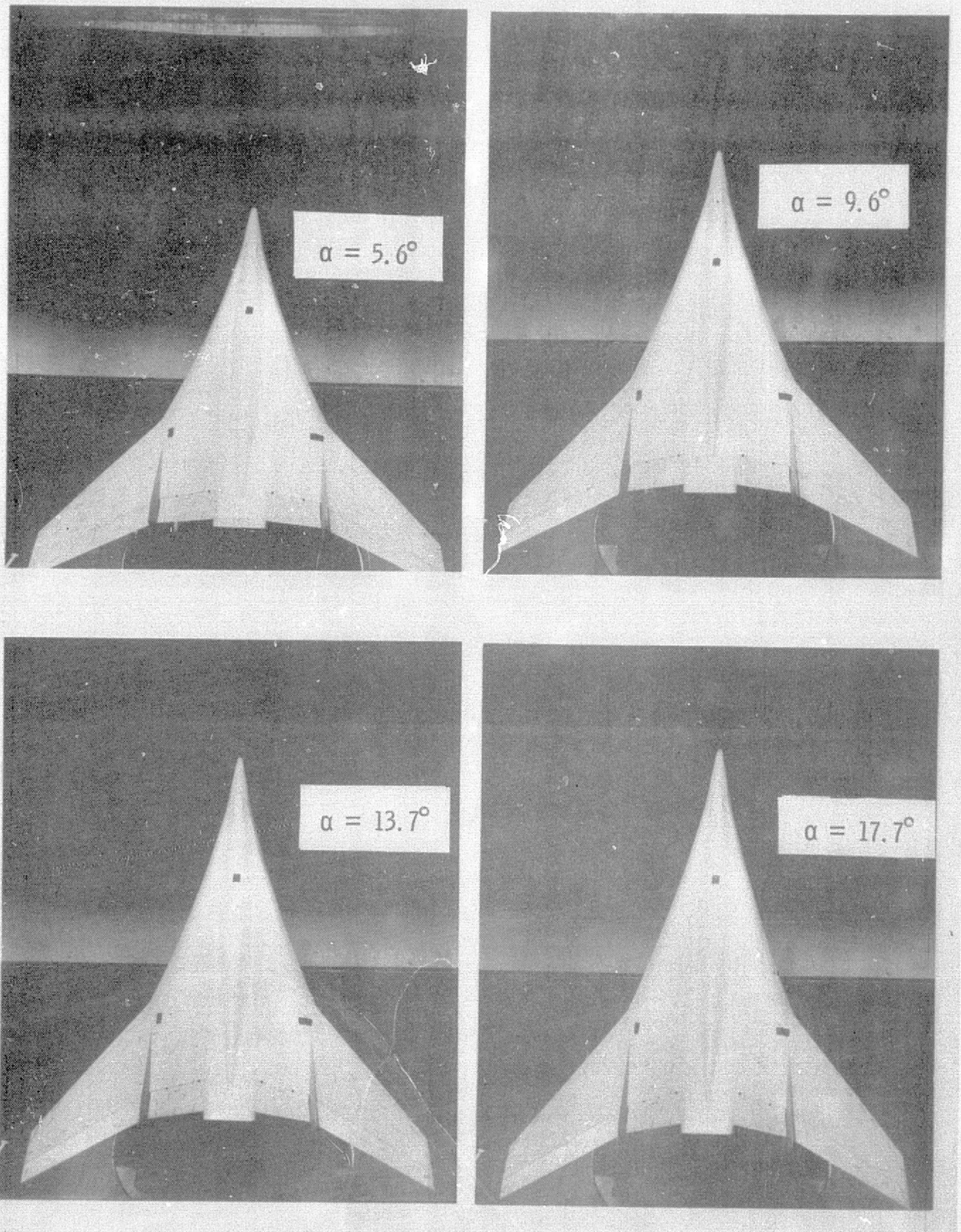

Figure 7. - Continued.

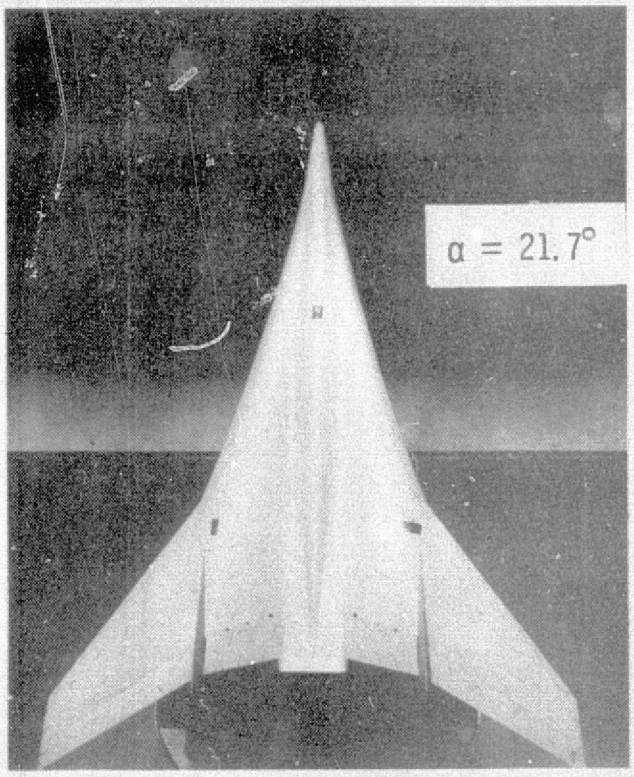

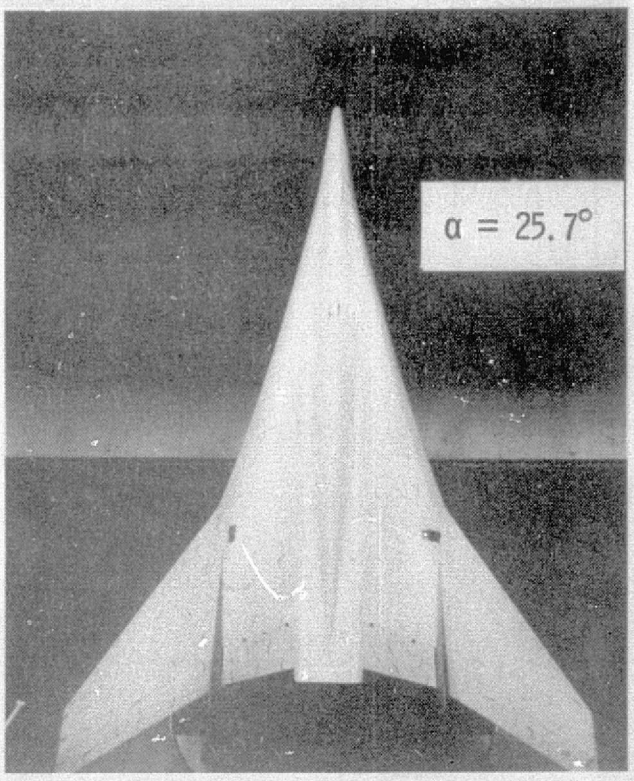

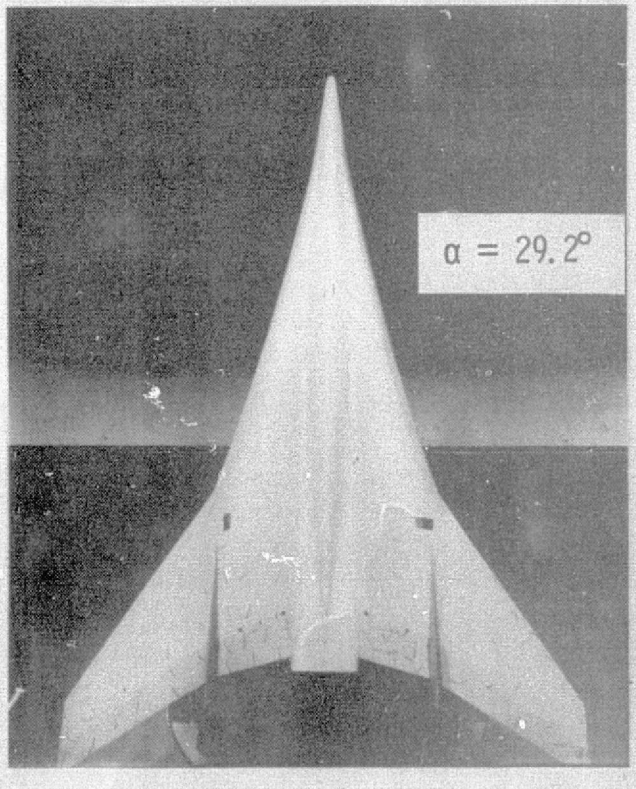

Figure 7. - Concluded.

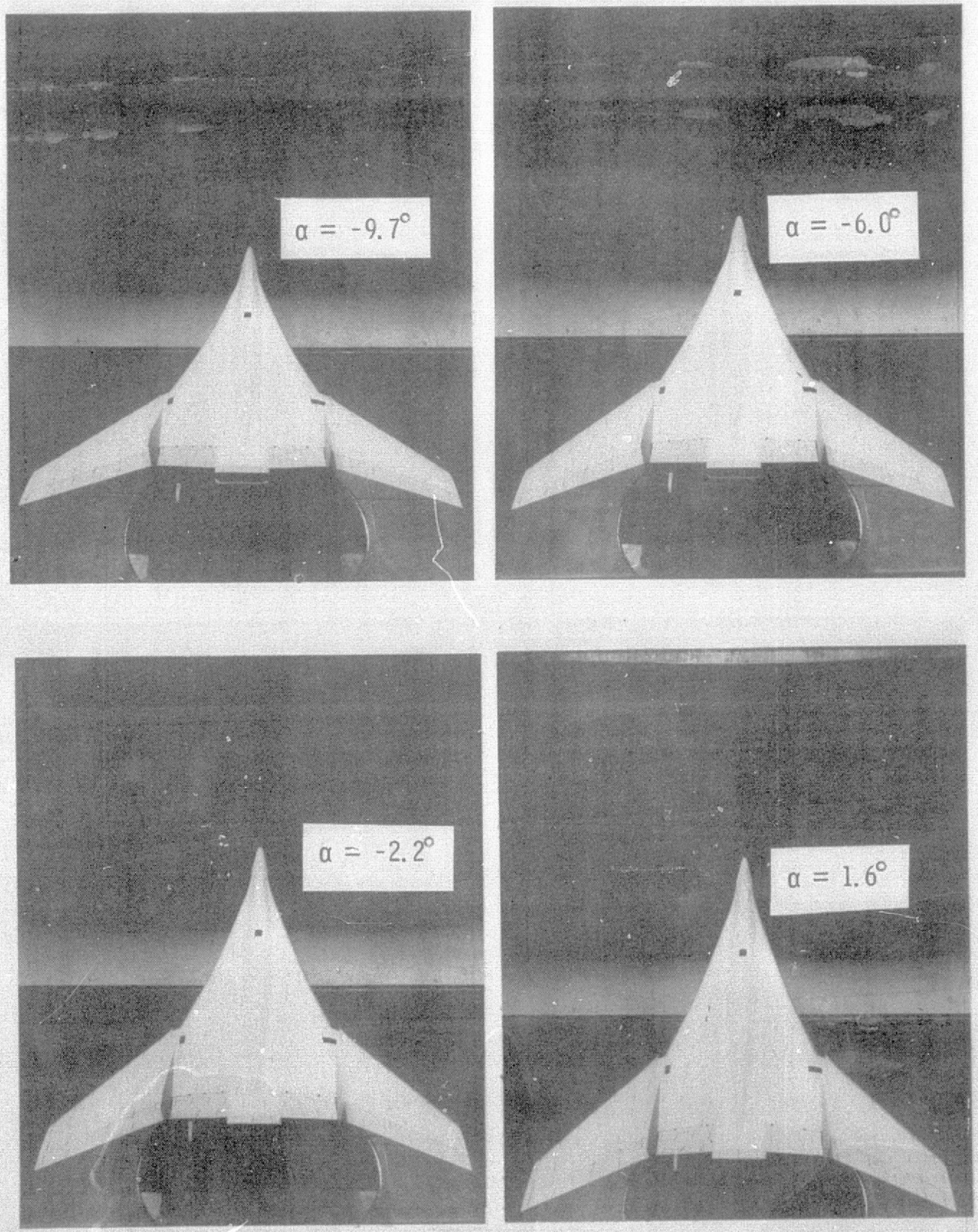

Figure 8. - Tuft photographs. $\delta_{n,\ 1,2,3} = 60°$. $\delta_f = 0°$ Krueger flap on, $C_\mu = 0$.

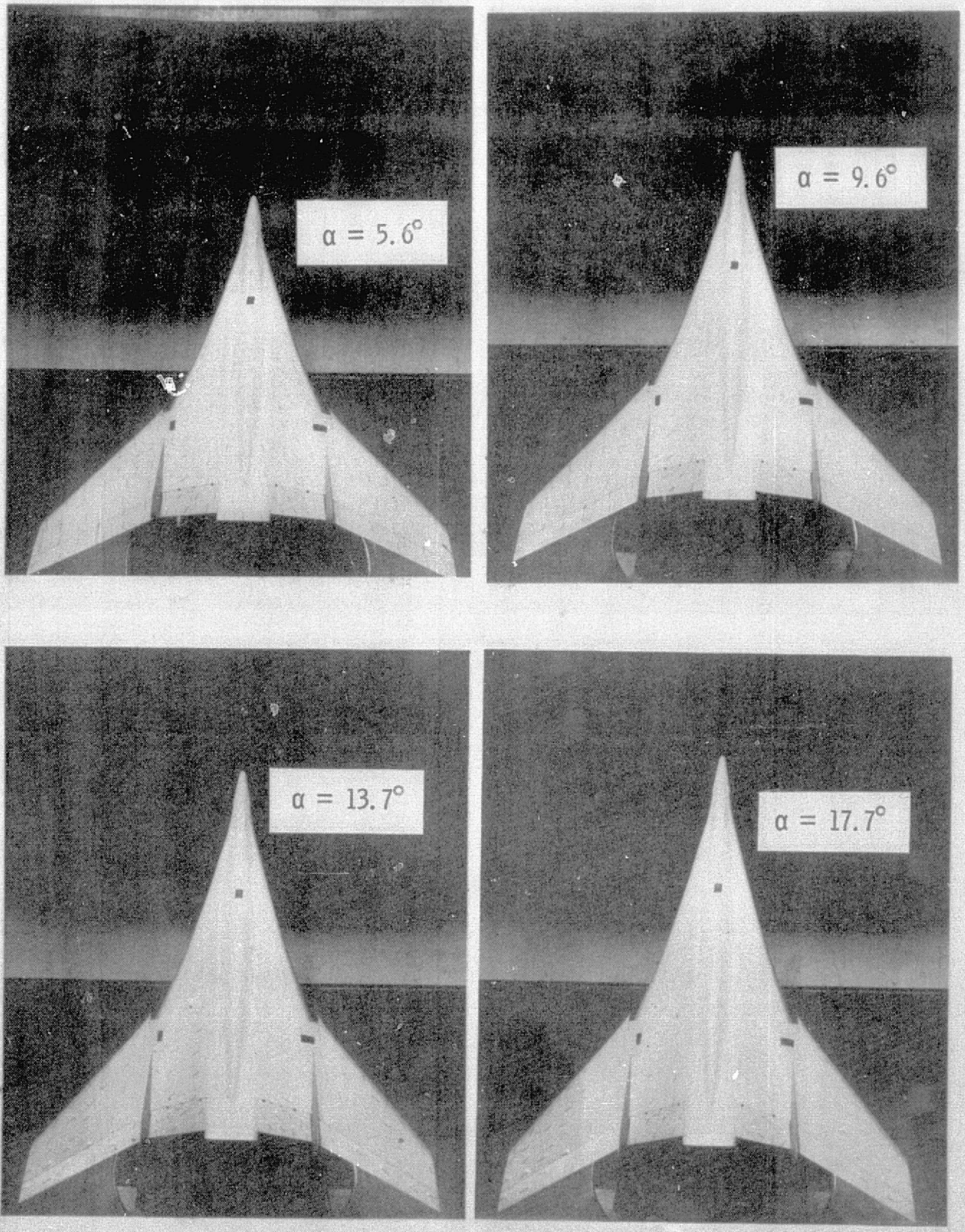

Figure 8. - Continued.

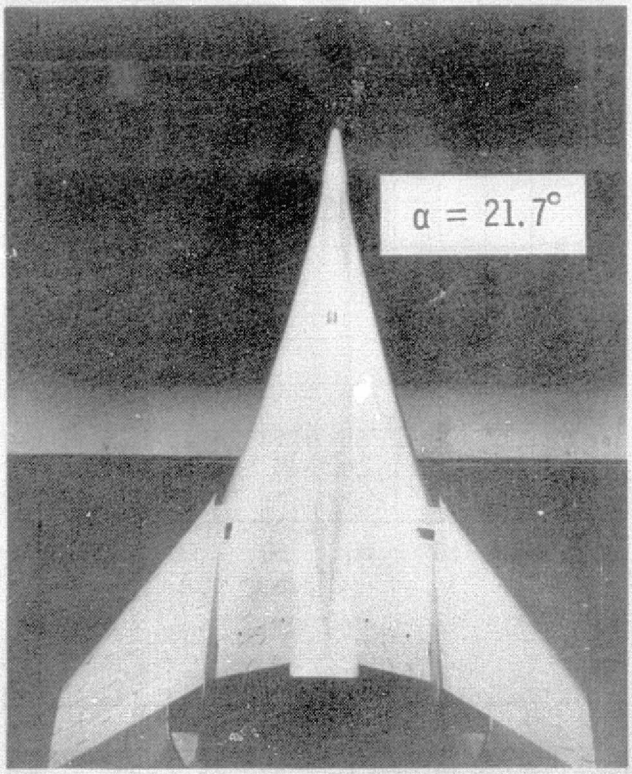

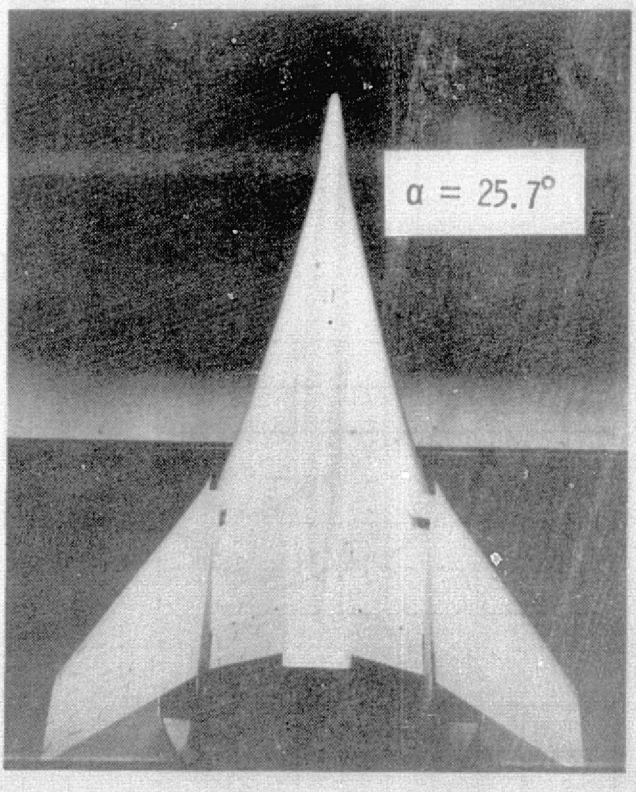

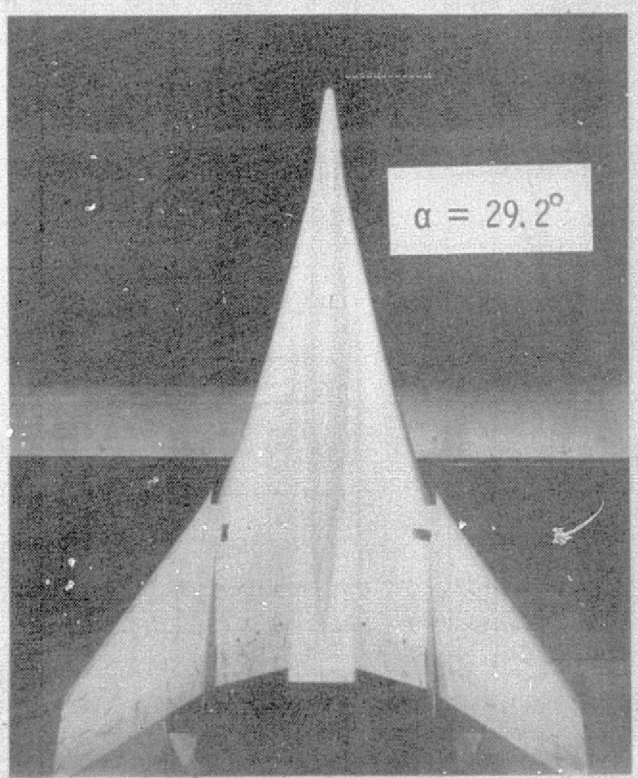

Figure 8. - Concluded.

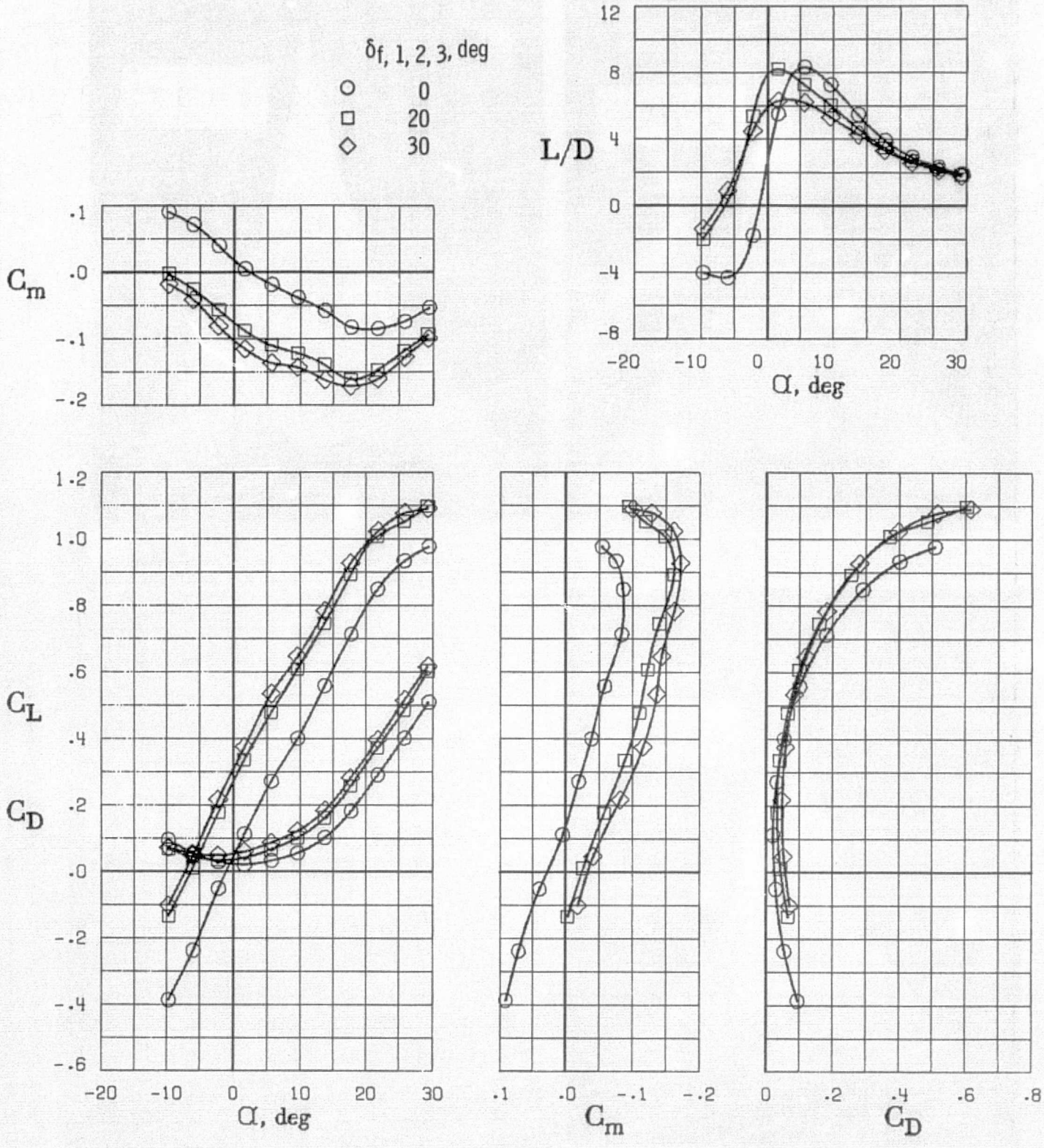

(a) Cruise engine mode.

Figure 9. - Effect of trailing-edge flap deflection. $\delta_{NOZ} = 0.^{\circ}$ $C_{\mu} = 0.$ $\delta_{n,1,2,3} = 60^{\circ}$. Krueger flap on.

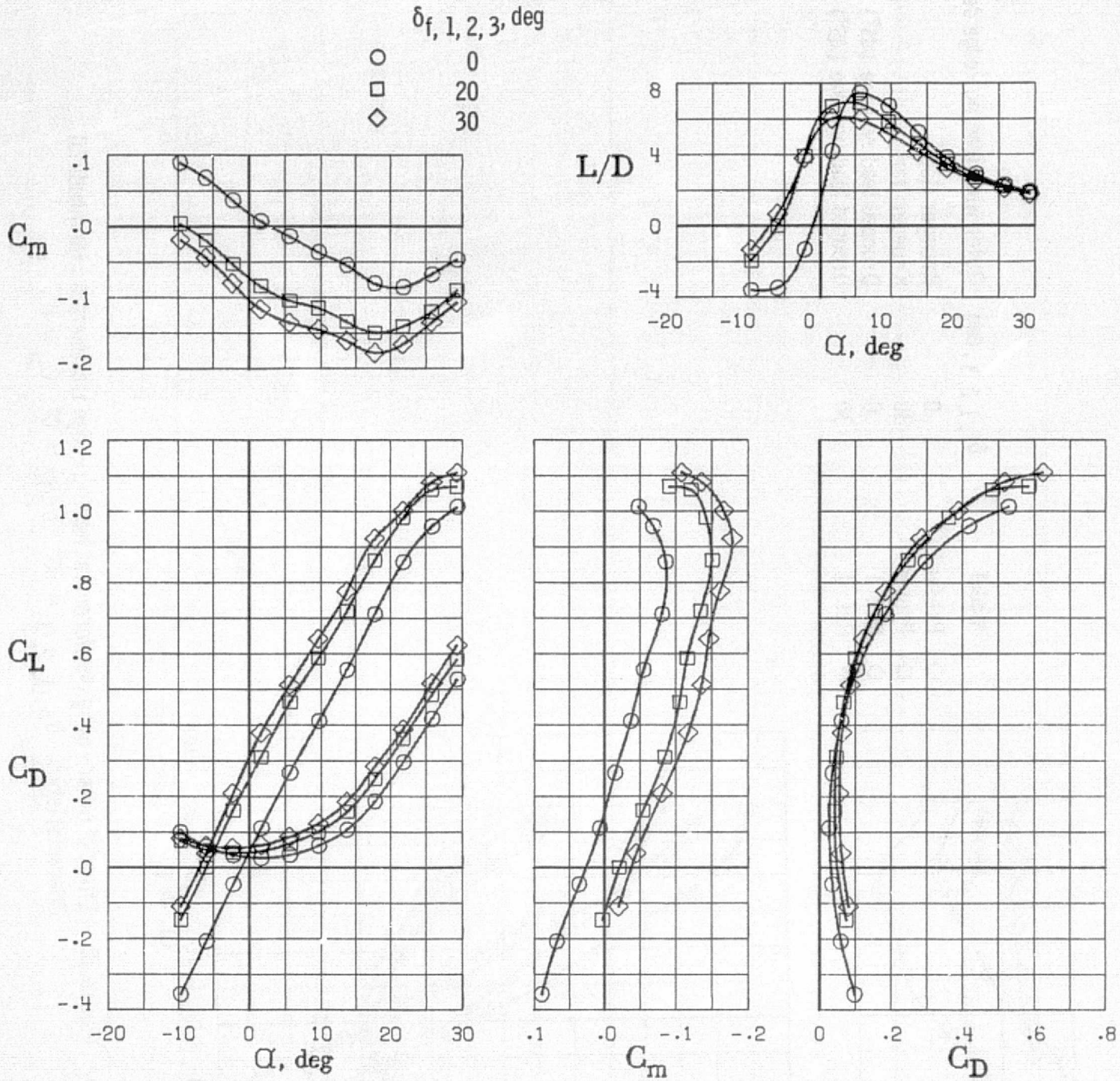

(b) Low-speed engine mode.

Figure 9. - Concluded.

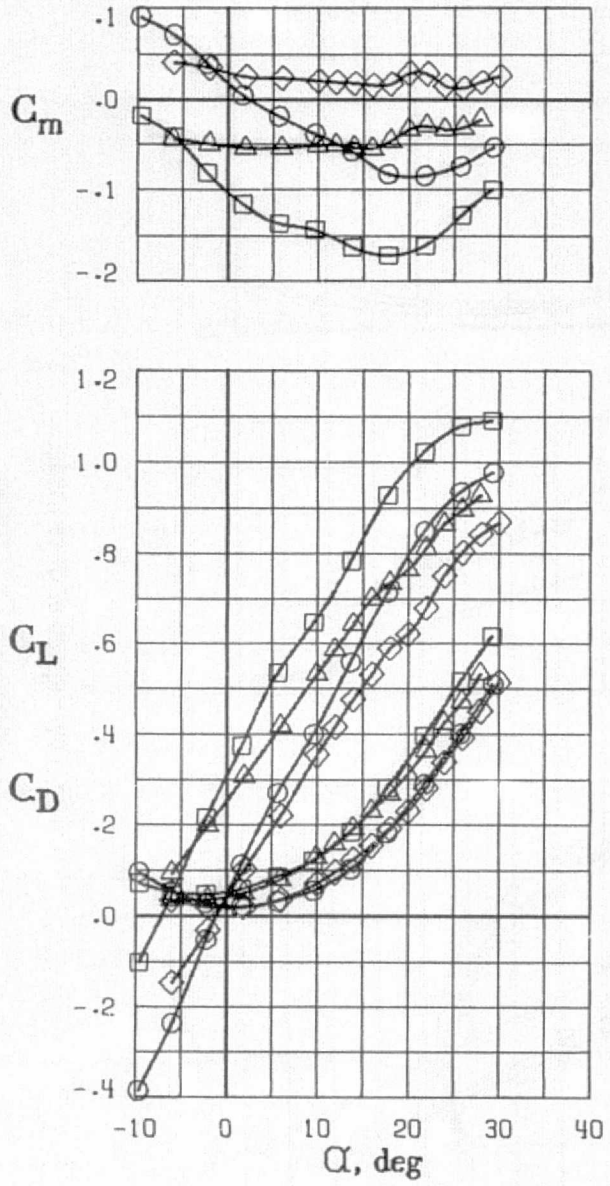

	Model	$\delta_{f,1,2,3}$, deg	Outer-wing leading-edge device
○	Present	0	Krueger flap
□	Present	30	Krueger flap
◇	Ref. 1	0	Drooped leading edge (45°)
△	Ref. 1	30	Drooped leading edge (45°)

Figure 10. - Effect of outer-wing planform and leading-edge treatment on longitudinal characteristics. $\delta_{n,1,2,3} = 60°$. $\delta_{NOZ} = 0°$. $C_\mu = 0°$.

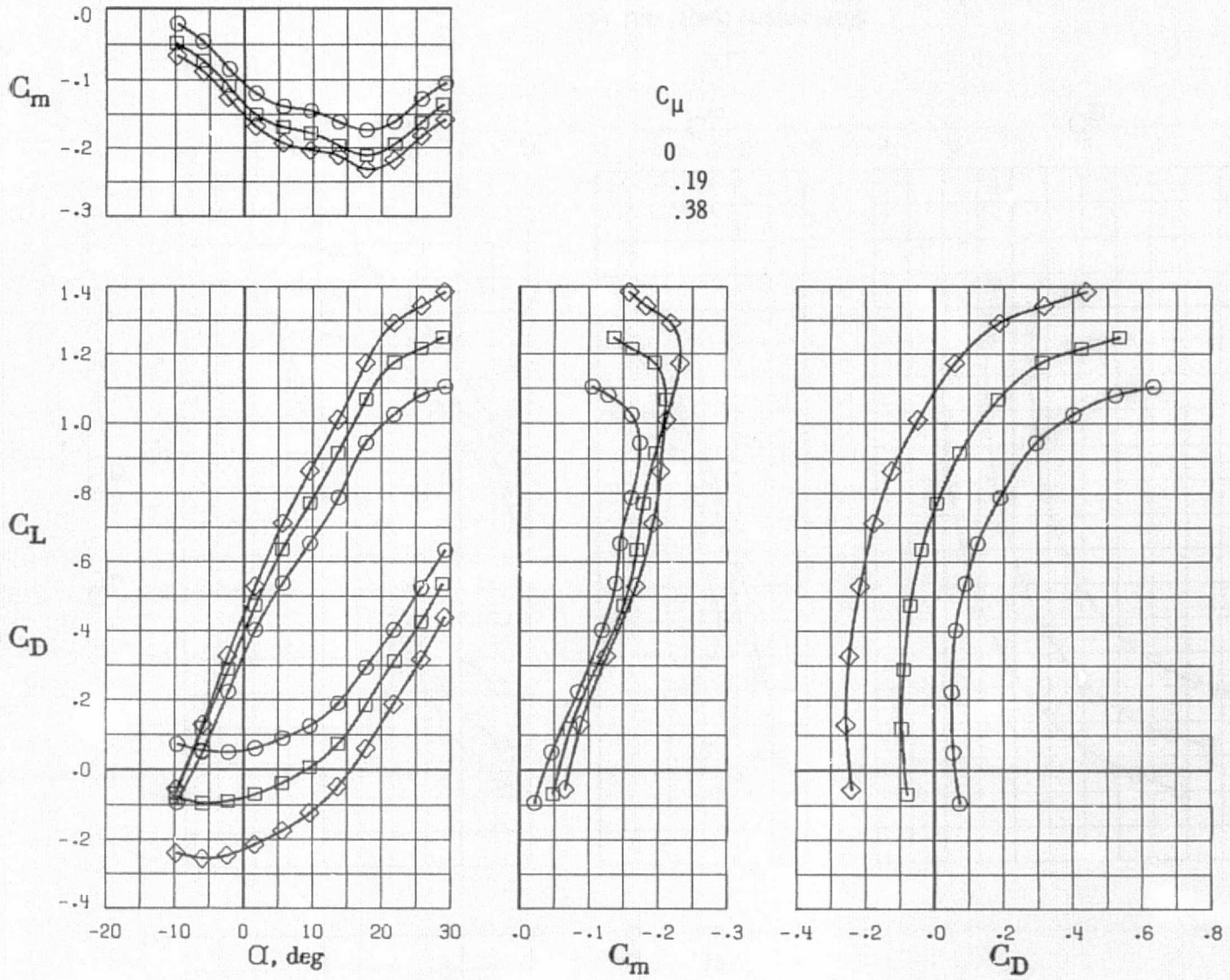

(a) Cruise engine mode.

Figure 11. - Effect of deflecting engine exhaust nozzle. $\delta_{n,1,2,3} = 60°$. $\delta_{f,1,2,3} = 30°$. Krueger flap on. $\delta_{NOZ} = 30°$.

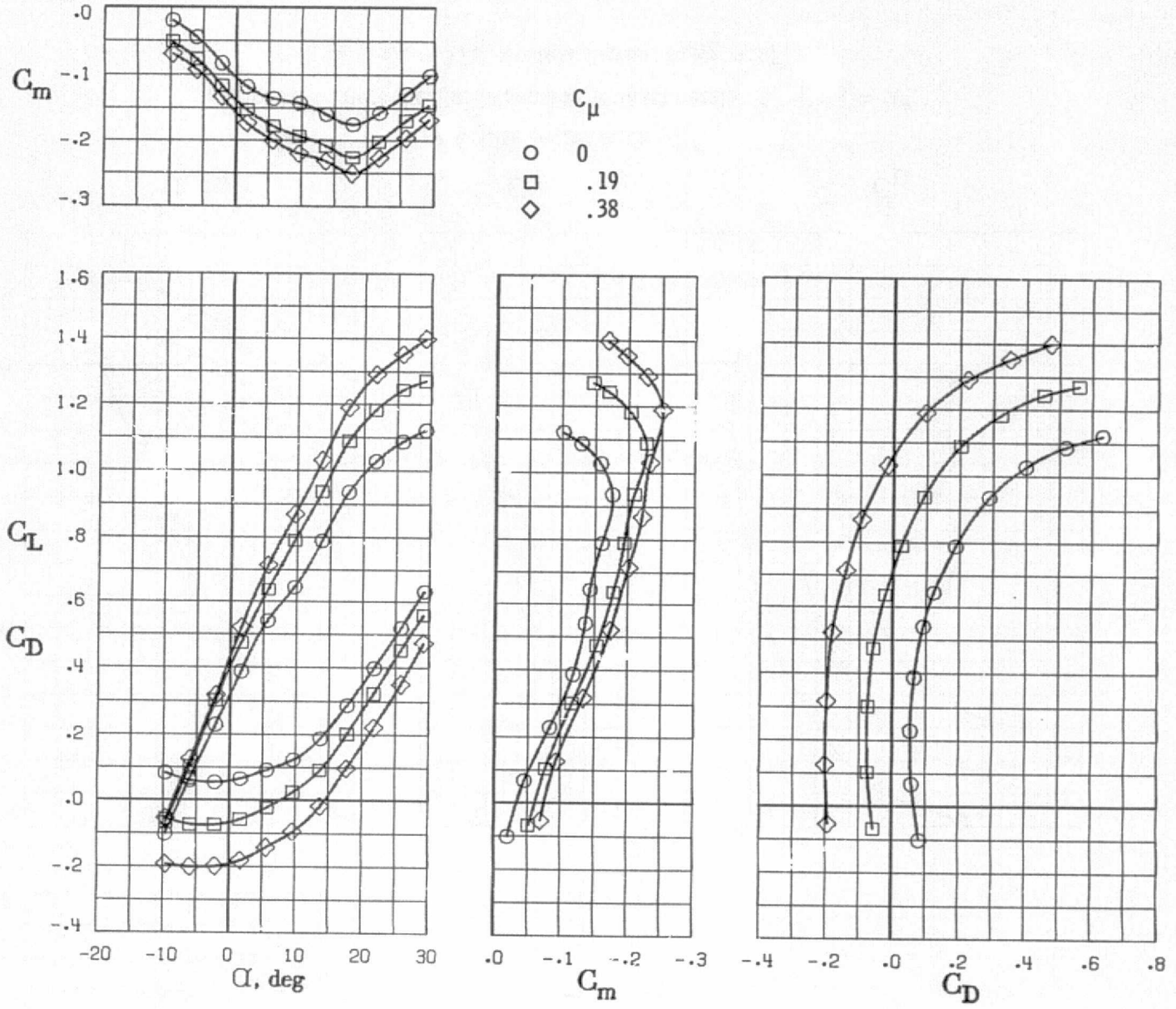

(b) Low-speed engine mode.

Figure 11. Concluded.

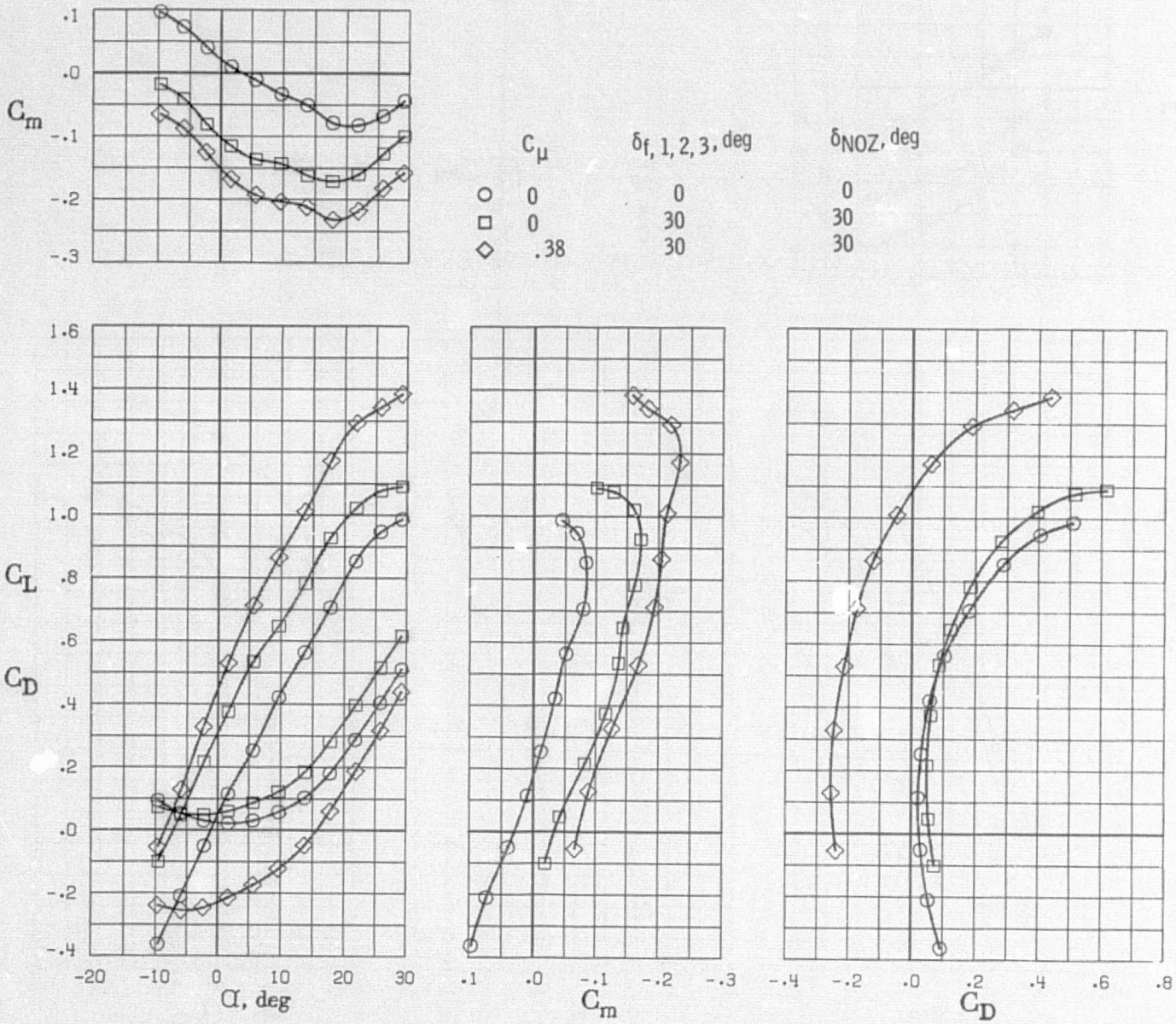

(a) Cruise engine mode.

Figure 12. - Individual contributions of flap and nozzle. $\delta_{n,1,2,3} = 60°$. Krueger flap on.

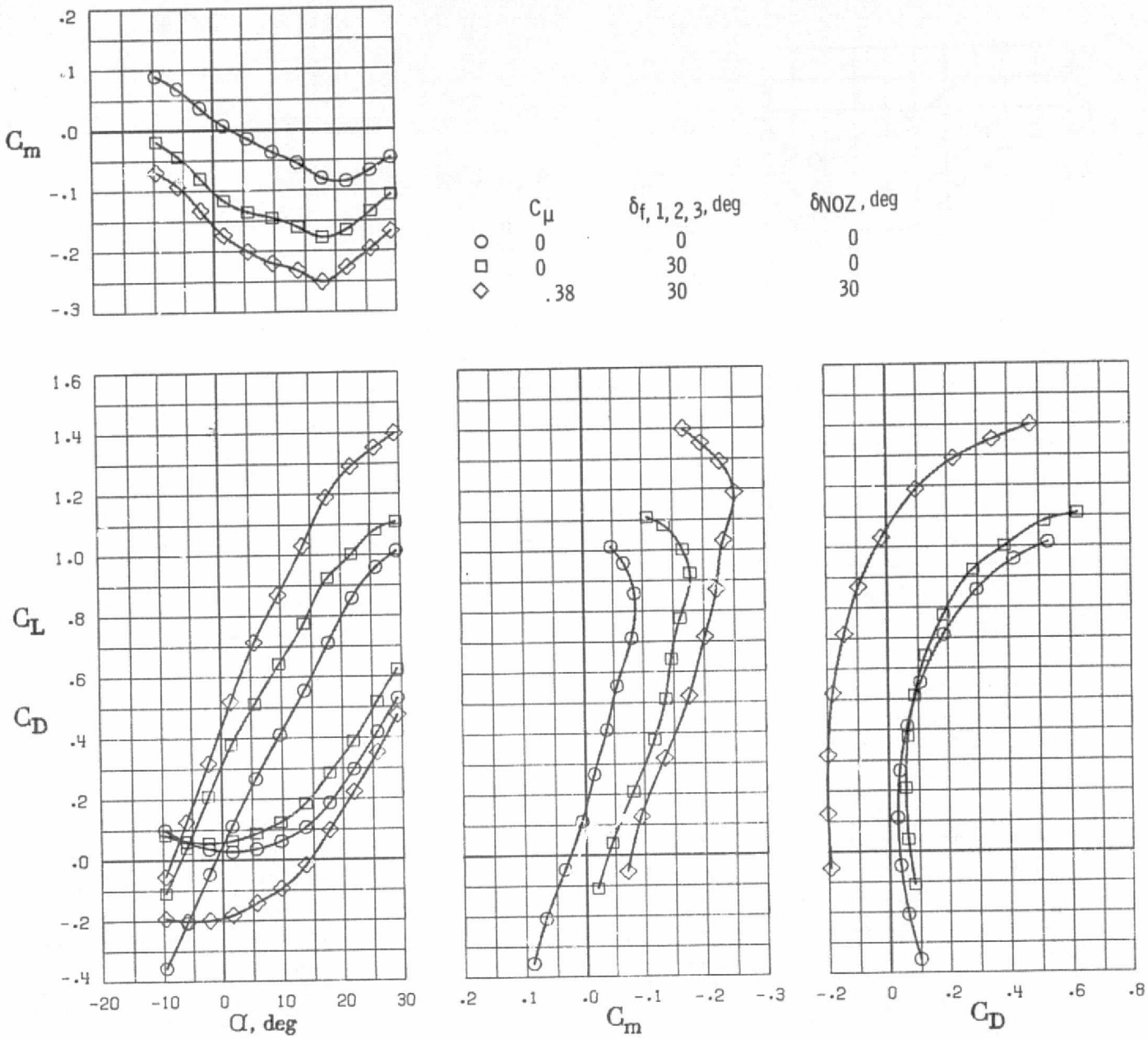

(b) Low-speed engine mode.

Figure 12. - Concluded.

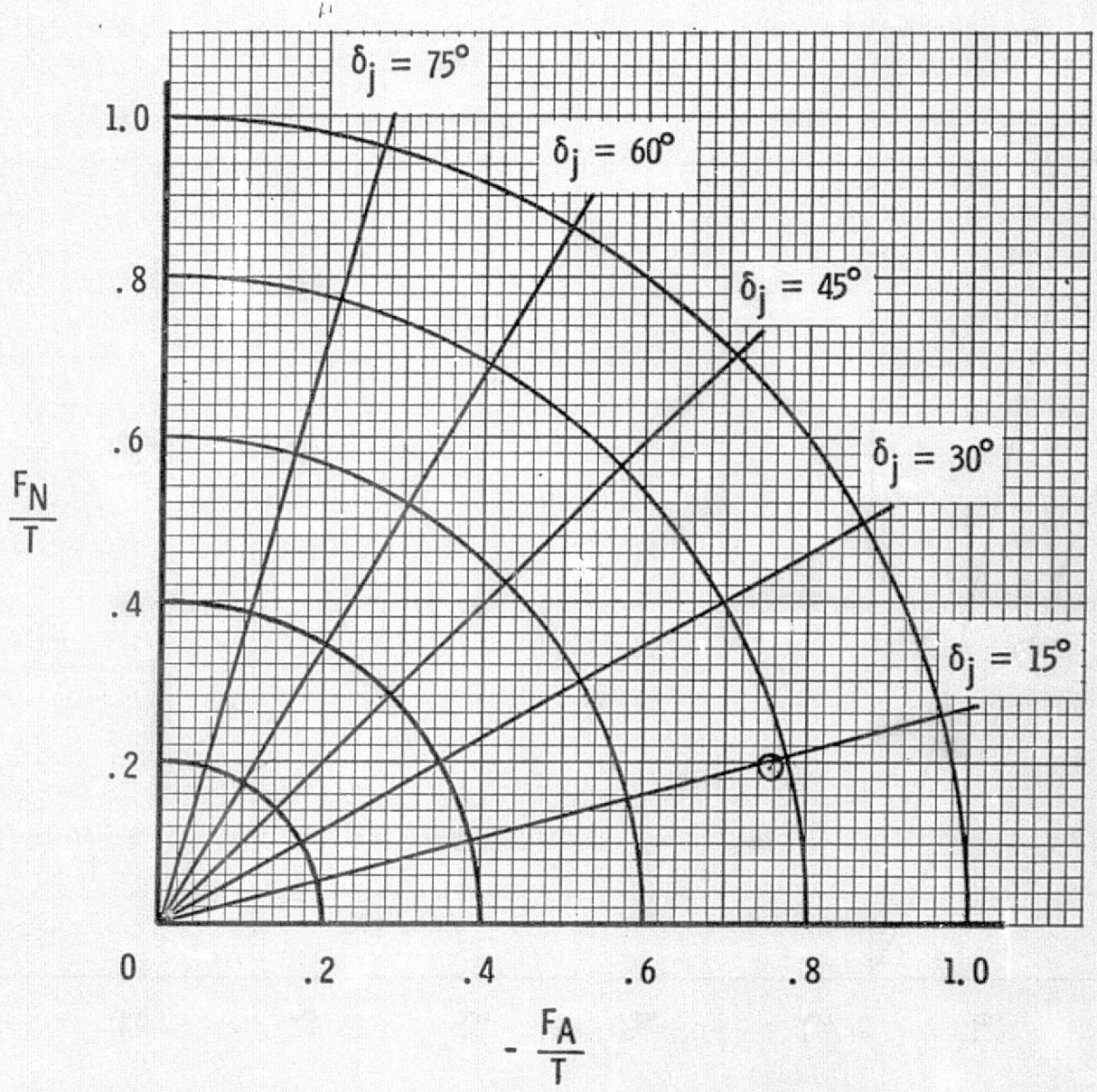

Figure 13. - Static turning and efficiency. $\delta_{NOZ} = 30°$. Low-speed engine mode. $\delta_f = 0°$.

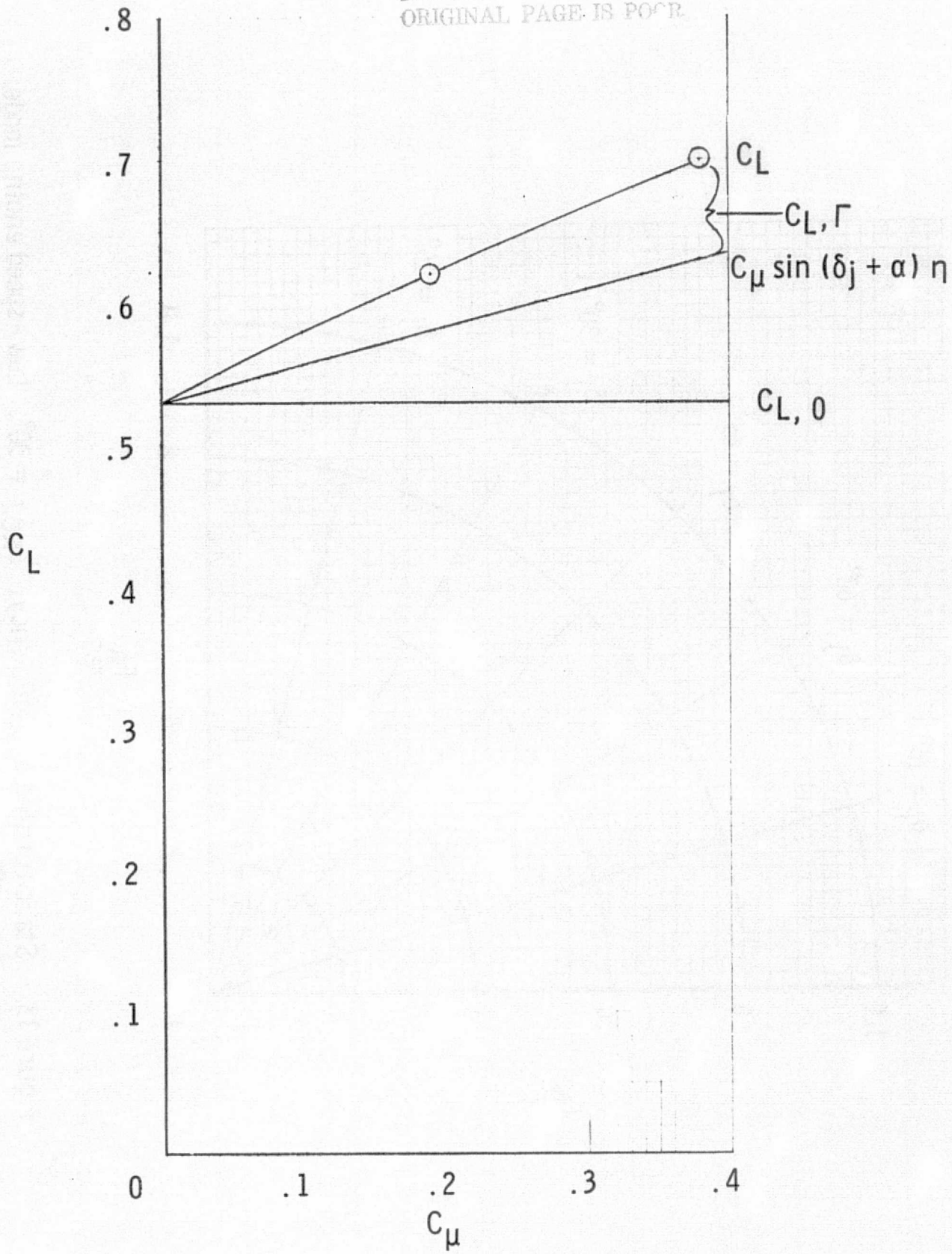

Figure 14. - Effectiveness of nozzle in producing added circulation lift. $\delta_{n,1,2,3} = 60°$. Krueger flap on. $\delta_{f,1,2,3} = 30°$. $\delta_{NOZ} = 30°$. Low speed engine mode. $\alpha = 5°$.

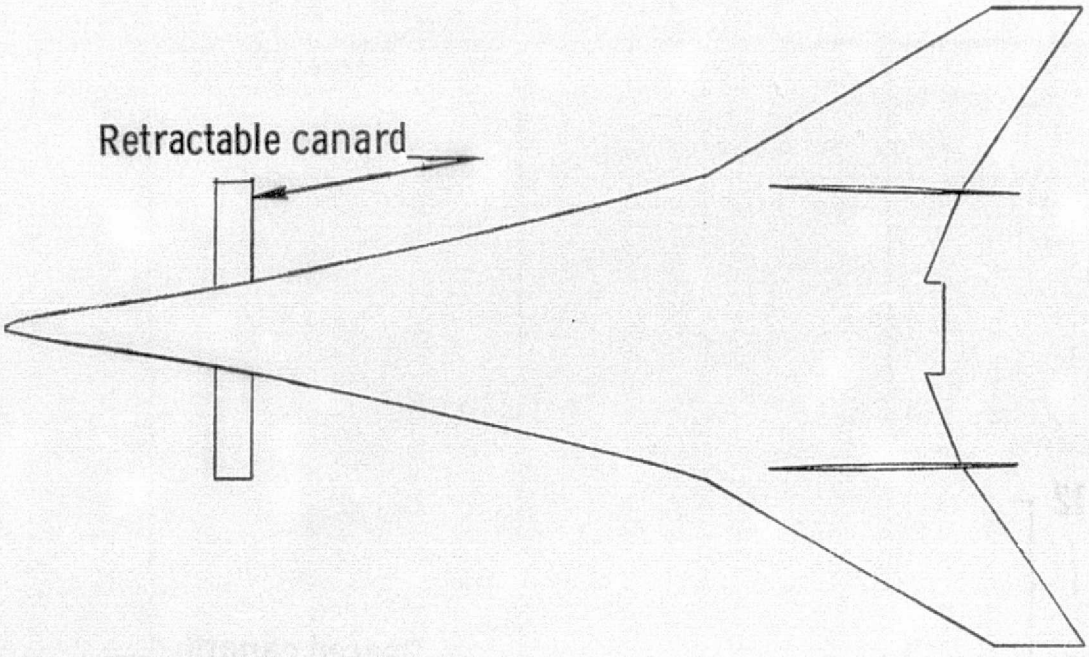

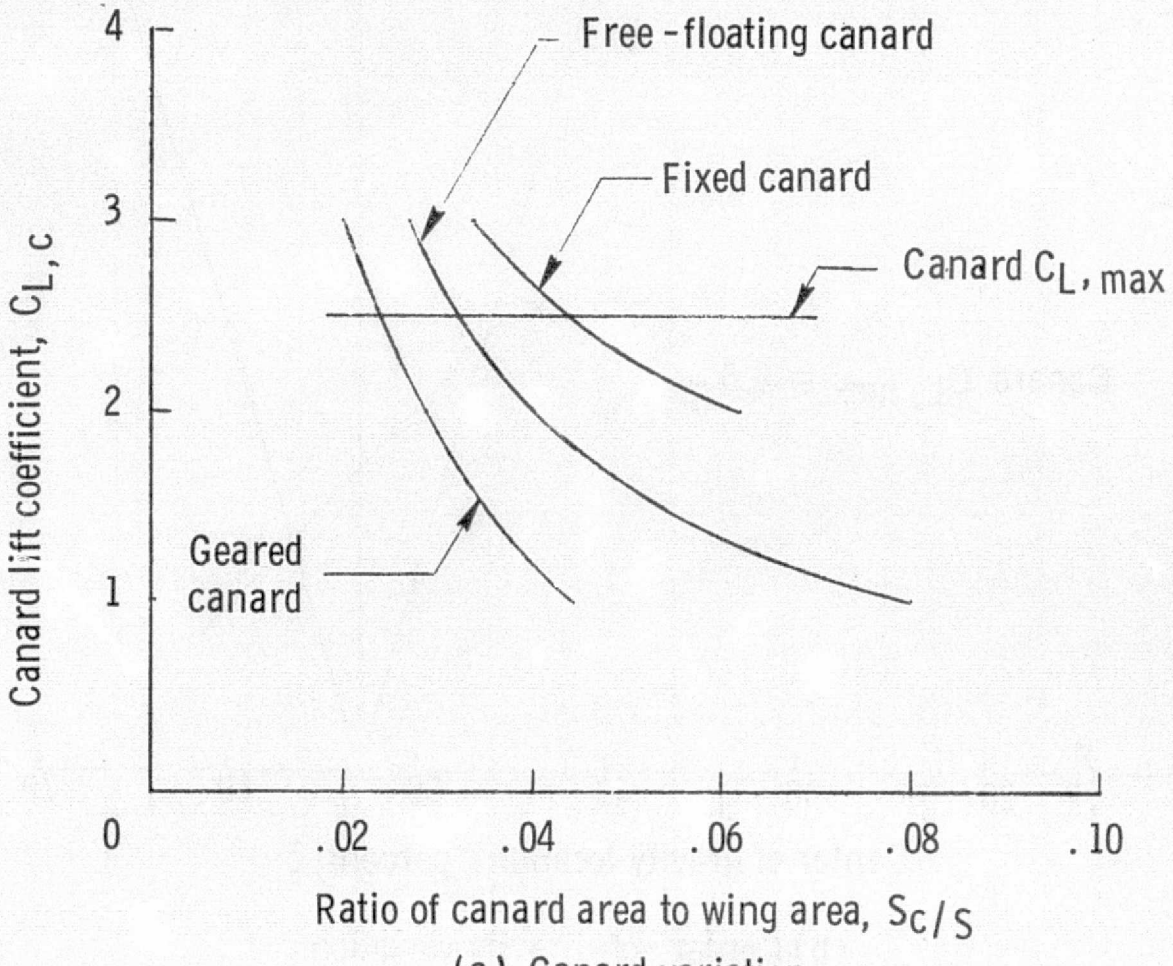

(a) Canard variation.

Figure 15. - Comparison of several methods of achieving pitch trim. $\delta_{f,1,2,3} = 30°$. Krueger flap on. $\delta_{NOZ} = 30°$. $\delta_{n,1,2,3} = 30°$. $C_\mu = 0.38$. $C_{L,trim} = 0.80$.

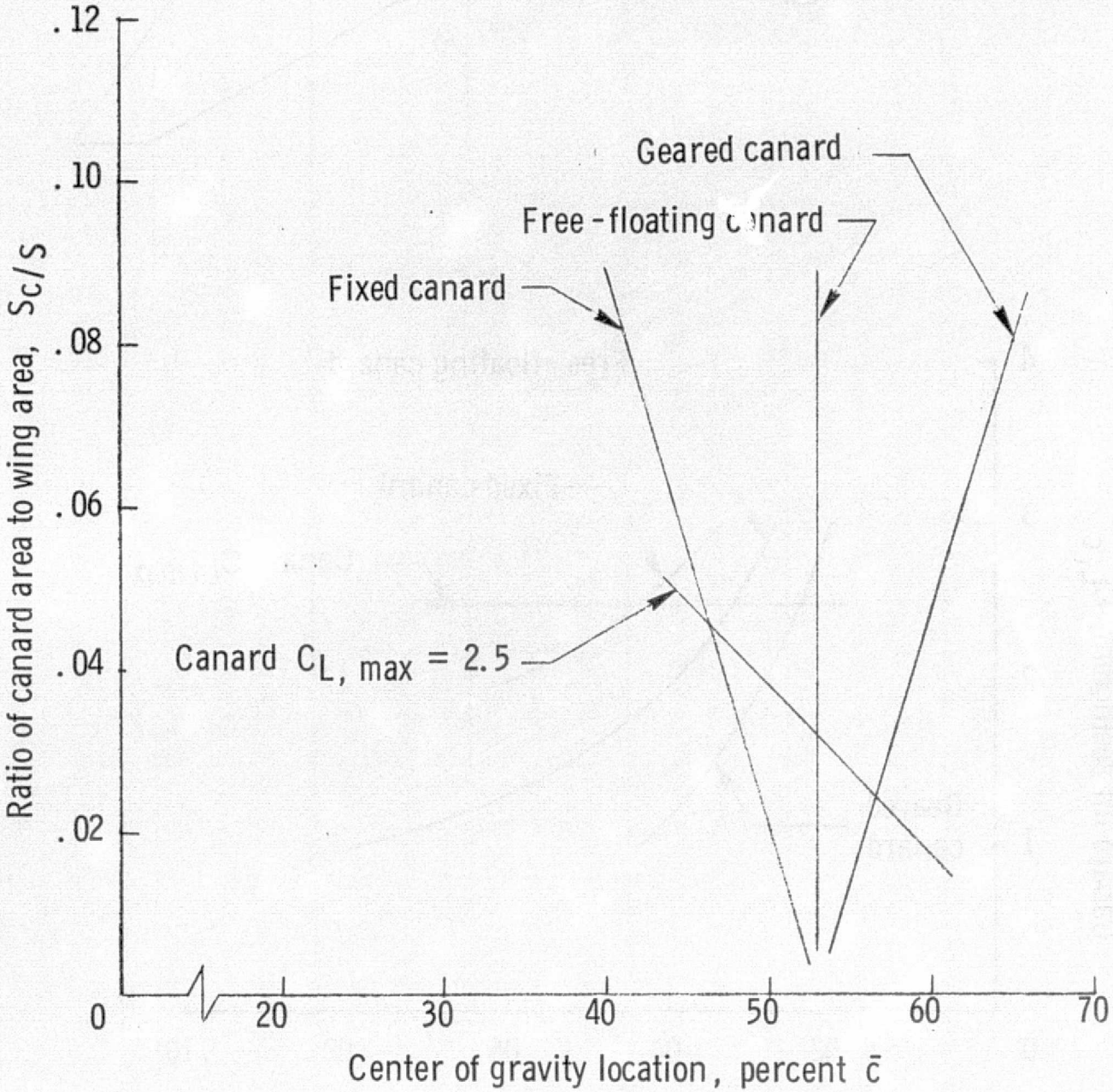

(b) Center-of-gravity variation.

Figure 15. - Concluded.

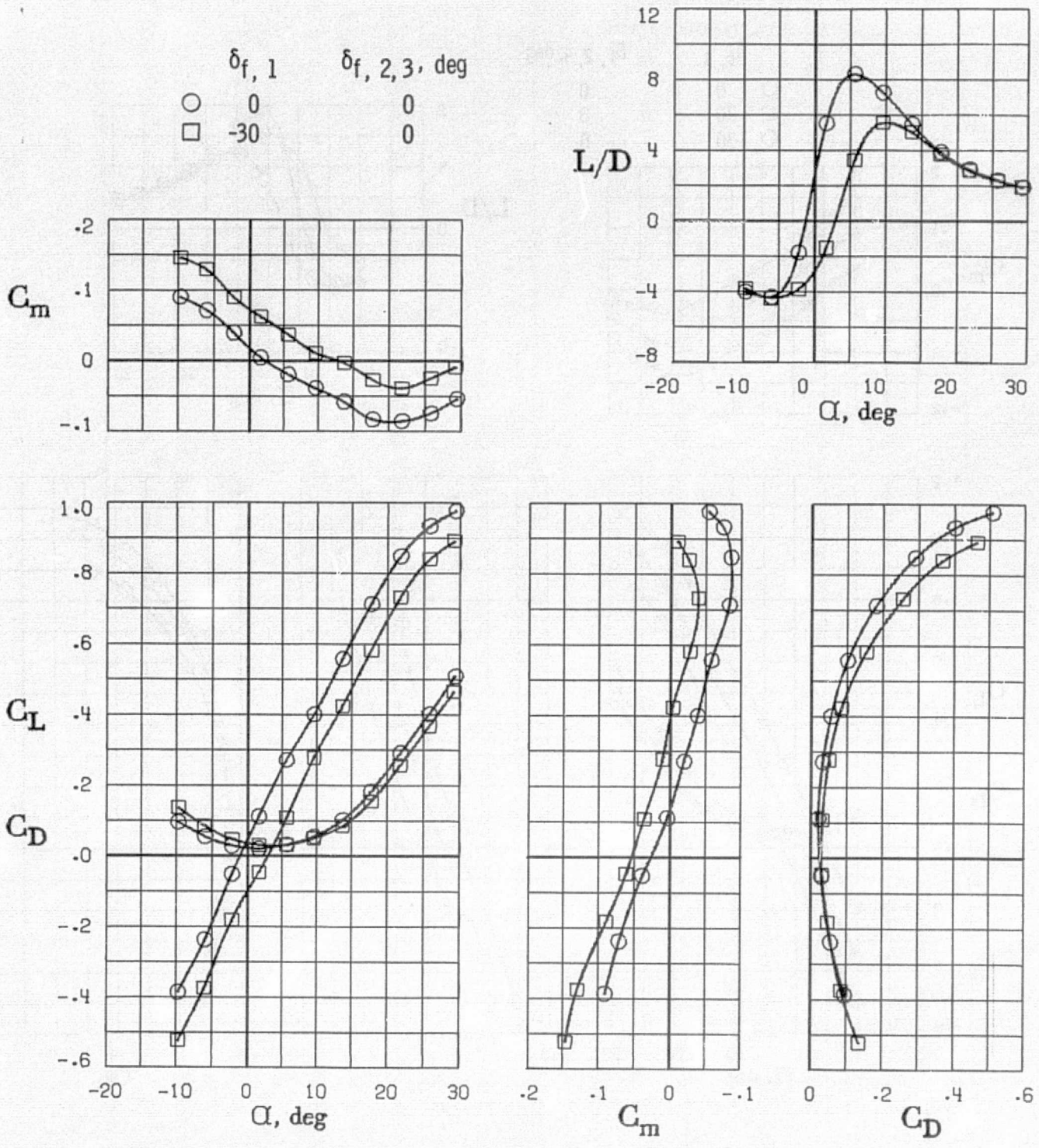

(a) Cruise engine mode.

Figure 16. - Effect of deflecting inboard segments of trailing-edge flap. $\delta_{n,1,2,3} = 60°$. $\delta_{NOZ} = 0°$. $C_\mu = 0$. Krueger flap on.

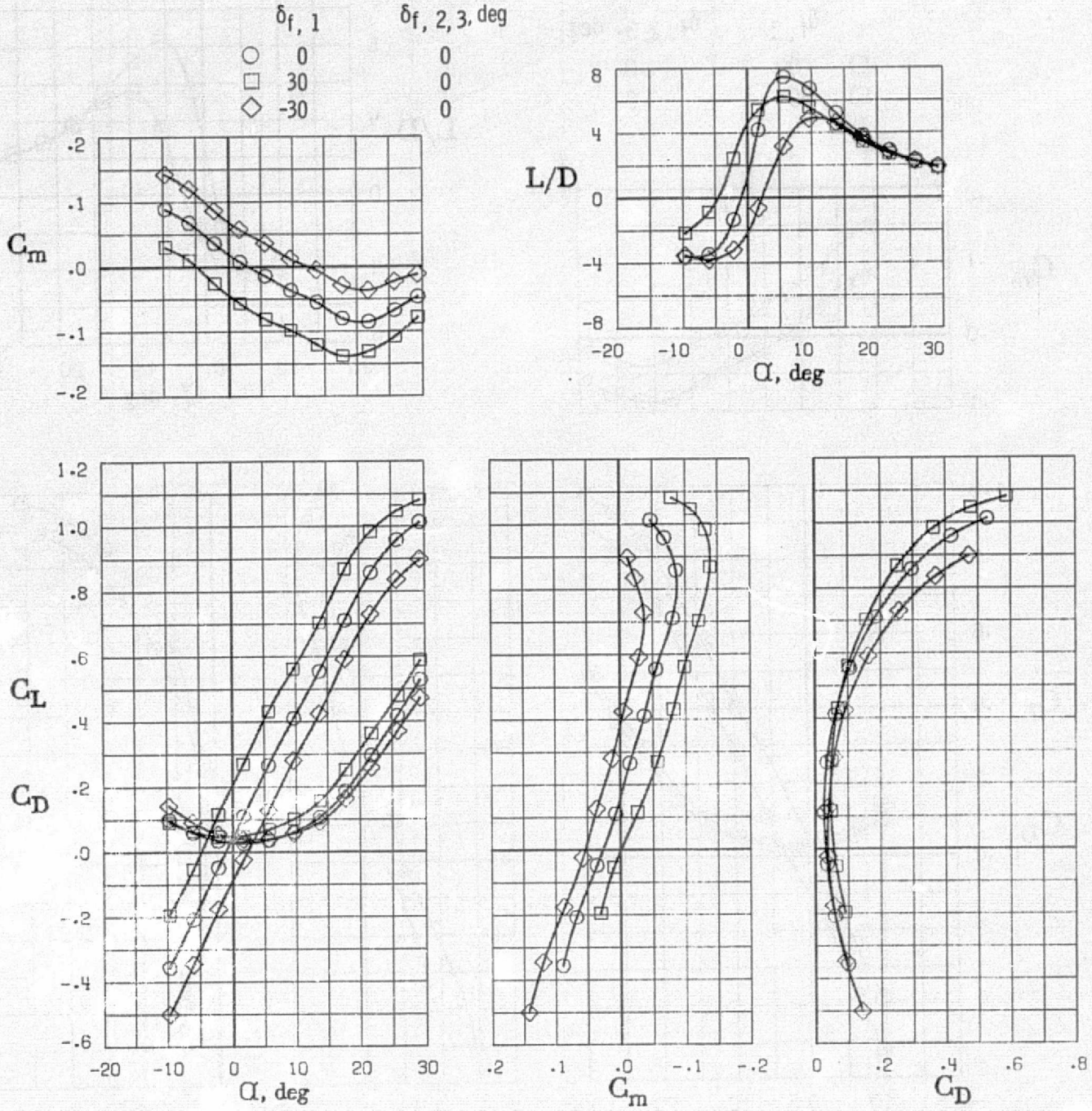

(b) Low-speed engine mode.

Figure 16. - Concluded.

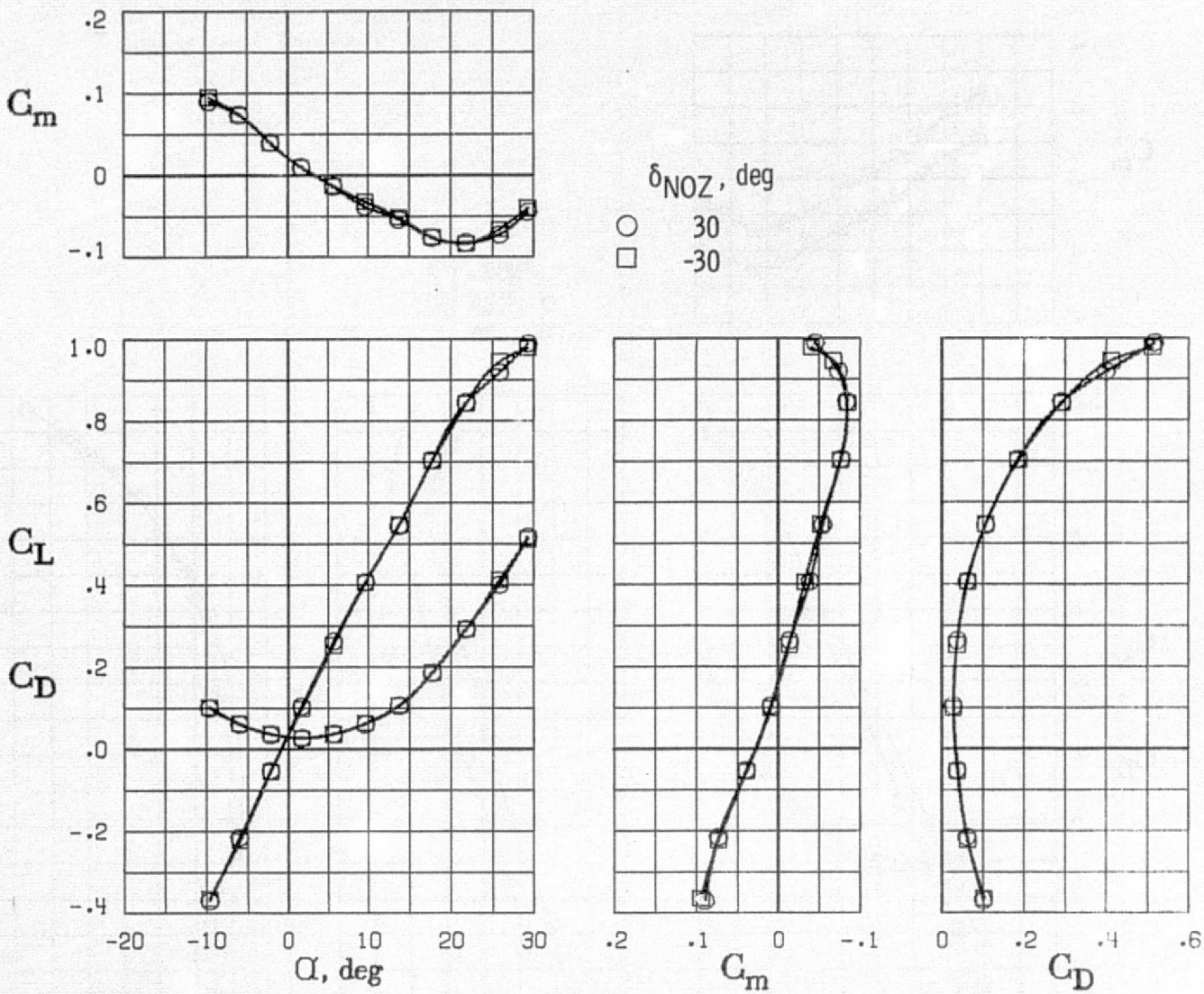

(a) $C_\mu = 0$.

Figure 17. - Effect of deflecting engine exhaust nozzle $\pm$ 30°. $\delta_{n,\,1,2,3} = 60°$. $\delta_{f,\,1,2,3} = 30°$. Low-speed engine mode. Wingtip Krueger on.

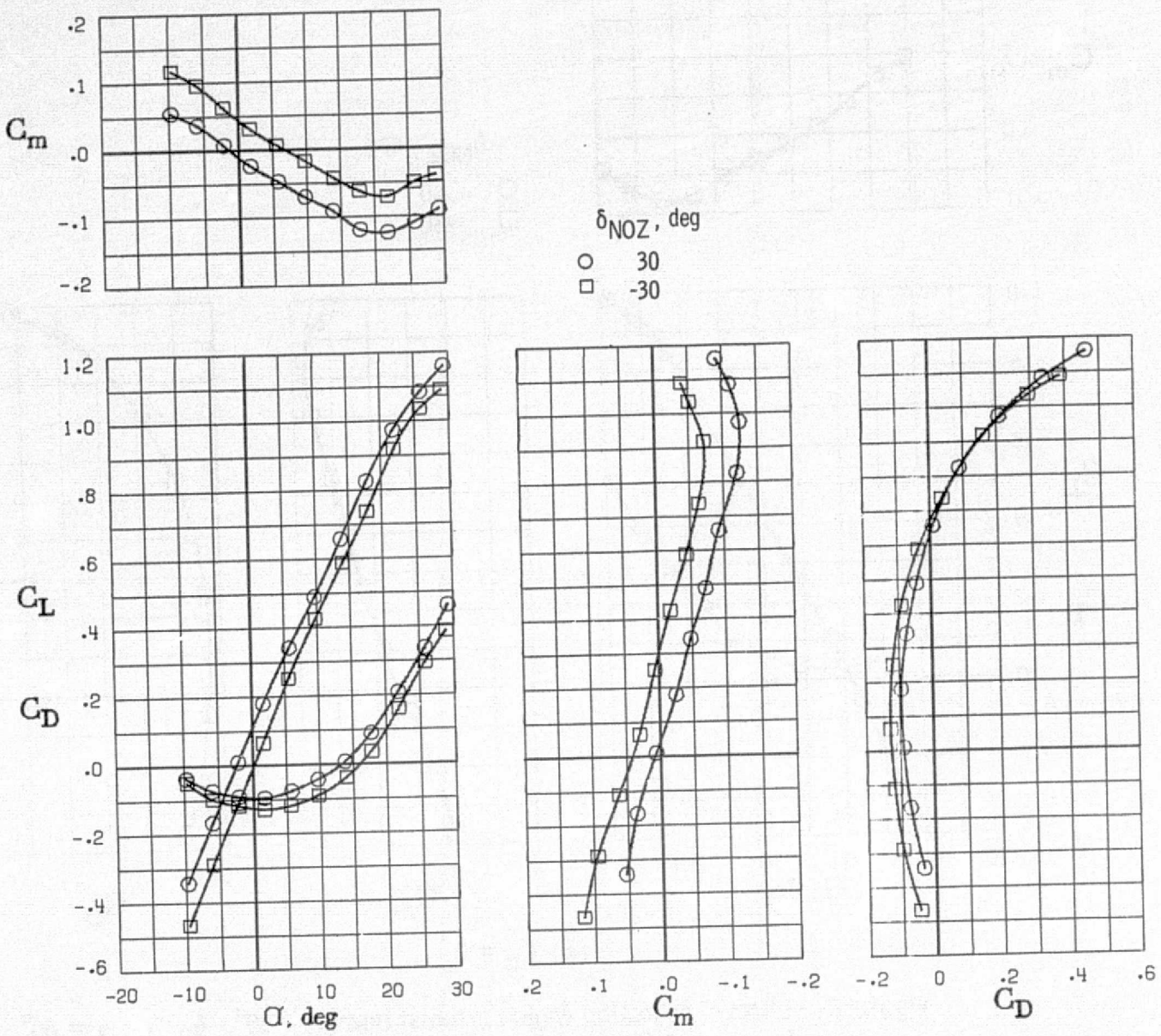

(b) $C_\mu = 0.19$

Figure 17. - Continued.

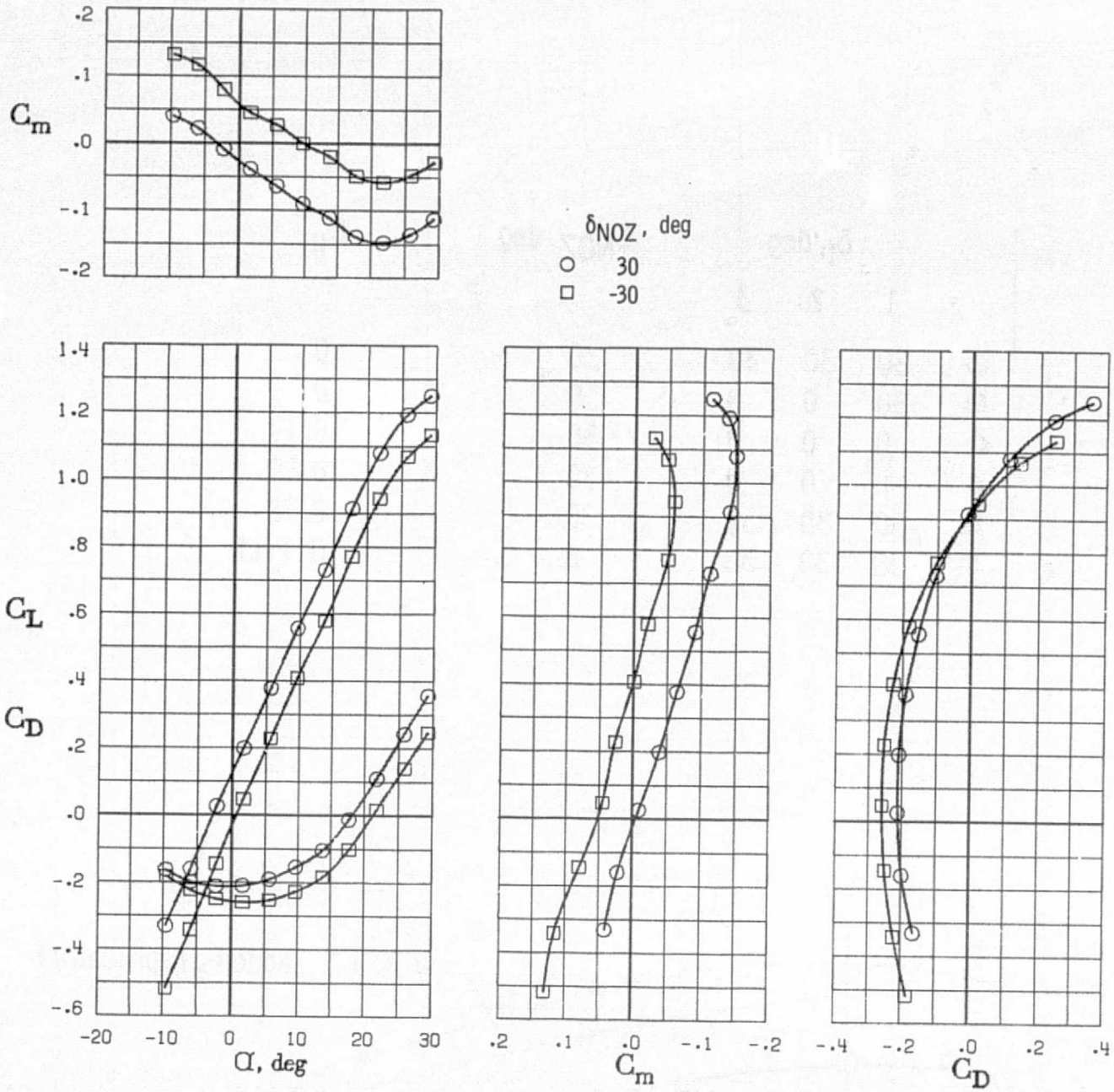

(c) $C_\mu = 0.38$

Figure 17. - Concluded.

	δ_f, deg			δ_{NOZ}, deg	C_μ
	1	2	3		
○	30	30	30	0	0
□	30	0	0	0	0
◇	0	0	0	30	0.19
△	0	0	0	30	0.38
◁	30	30	30	30	0.38
▷	30	30	30	0	0 (ref. 1)

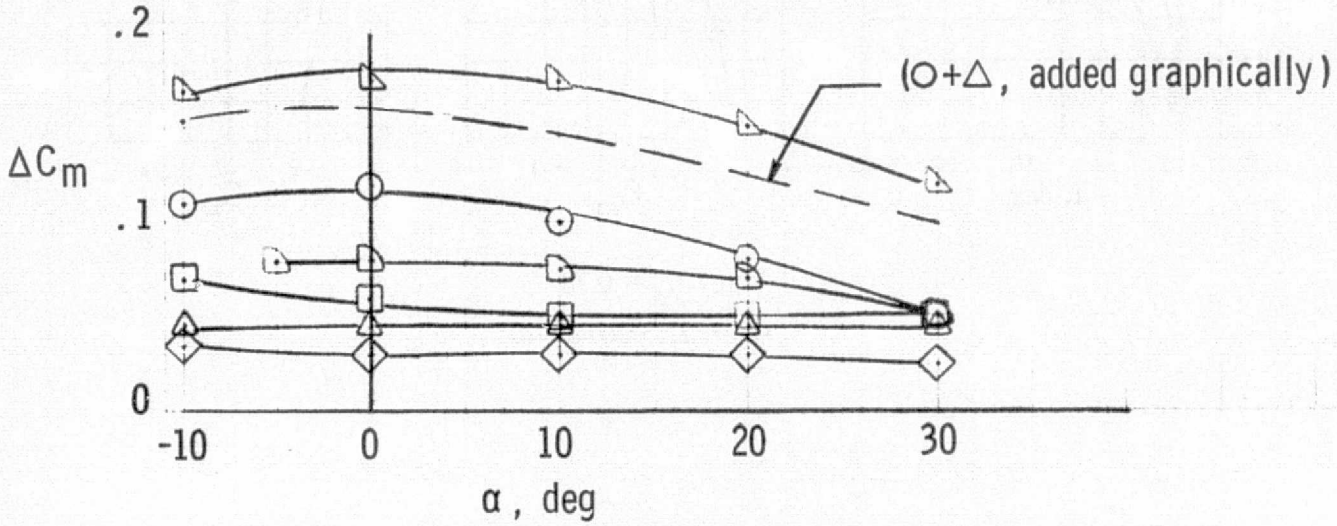

Figure 18. - Comparison of longitudinal control effectiveness produced by deflection of various trailing-edge control devices. $\delta_{n,1,2,3} = 60°$. Krueger on.

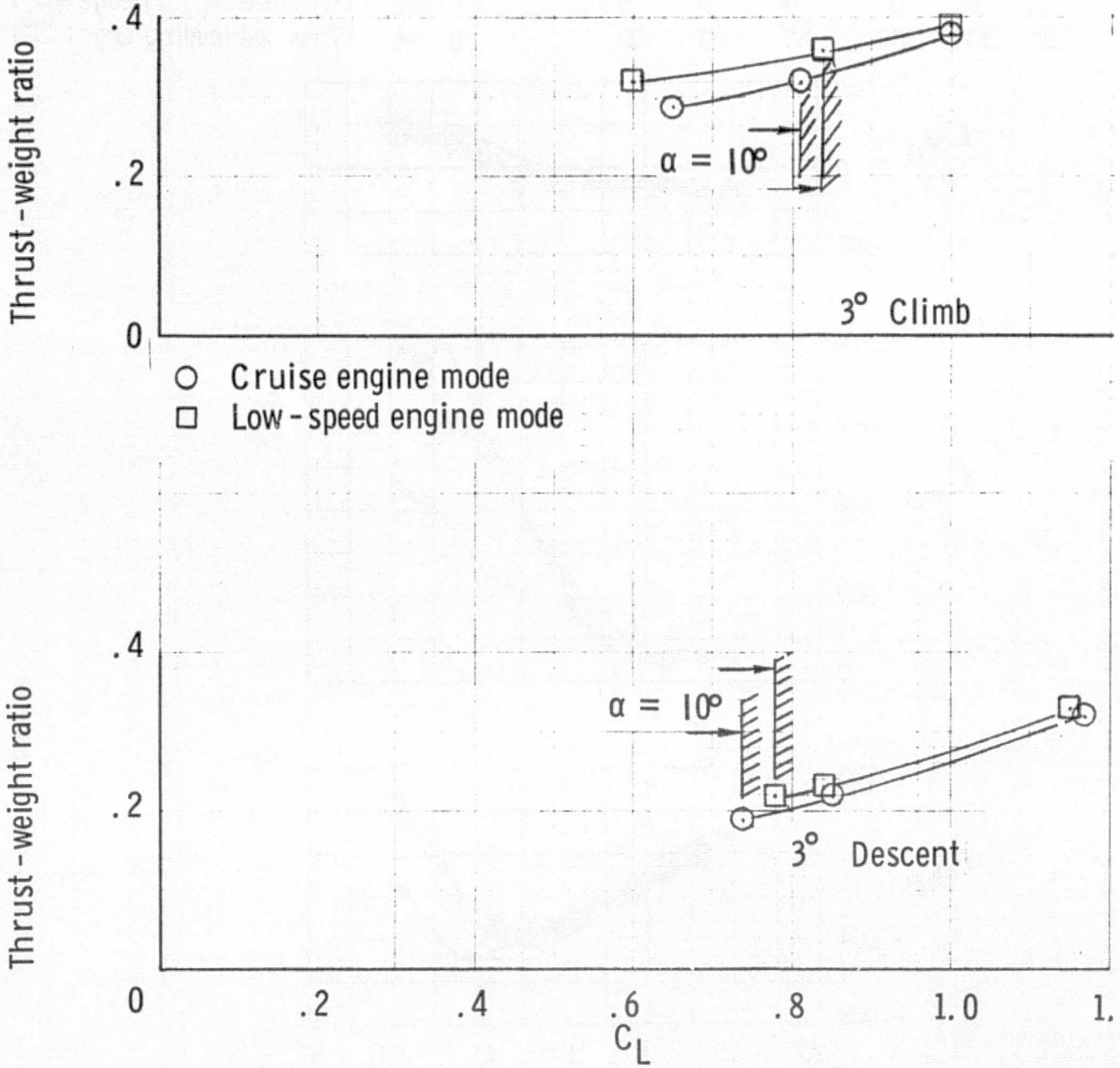

Figure 19. - Effect of variable - cycle engine mode on T/W vs C_L for climb and descent conditions. $\delta_{f,1,2,3} = 30°$; $\delta_{n,1,2,3} = 30°$, $\delta_{NOZ} = 30°$; Krueger on.

	δ_f, deg			δ_n, deg			C_μ	Outer-wing leading-edge device
	1	2	3	1	2	3		
○	0	0	0	60	60	60	0	Krueger flap
◇	0	0	0	60	60	60	0.19	Krueger flap
△	0	0	0	0	0	0	0 (ref. 1)	Drooped leading edge (45°)
◁	30	30	30	60	60	60	0 (ref. 1)	Drooped leading edge (45°)

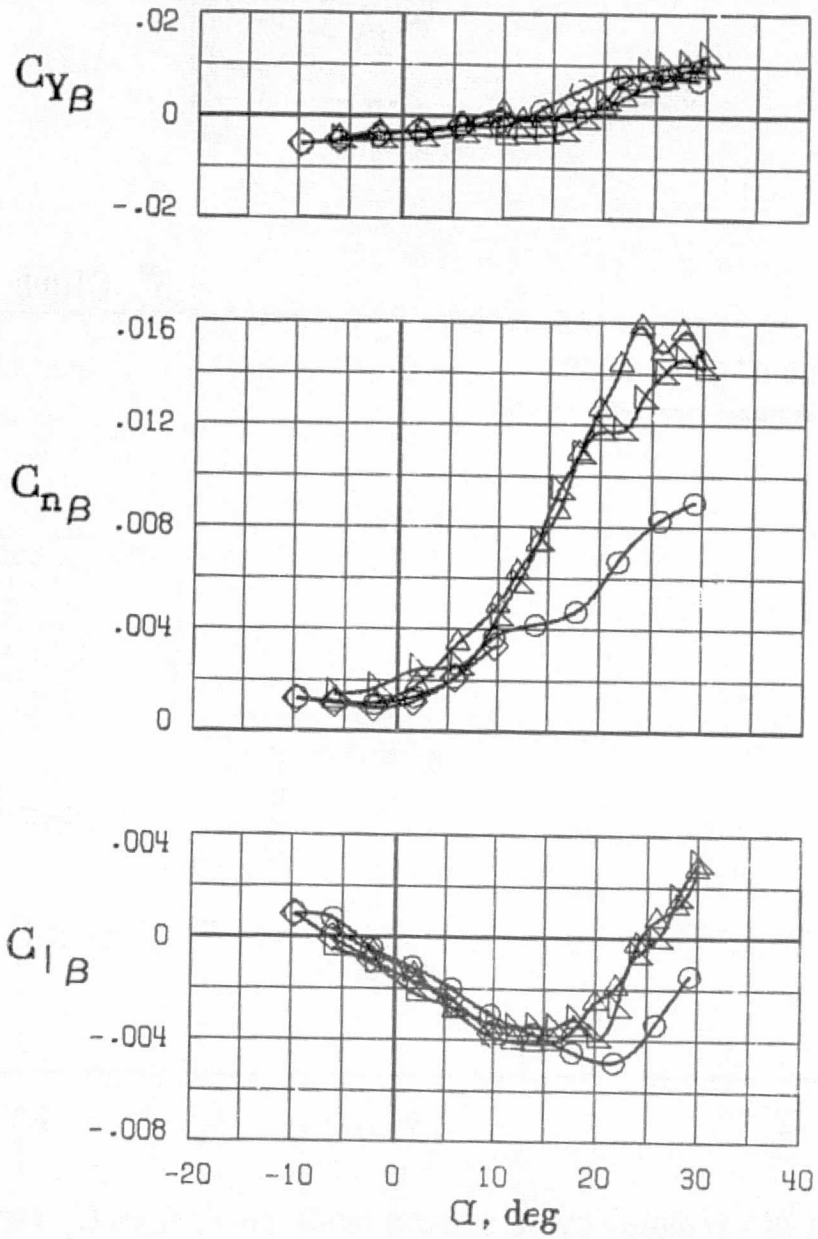

(a) Cruise engine mode.

Figure 20. - Variation of lateral-directional stability derivatives with angle of attack. $\delta_{NOZ} = 0°$.

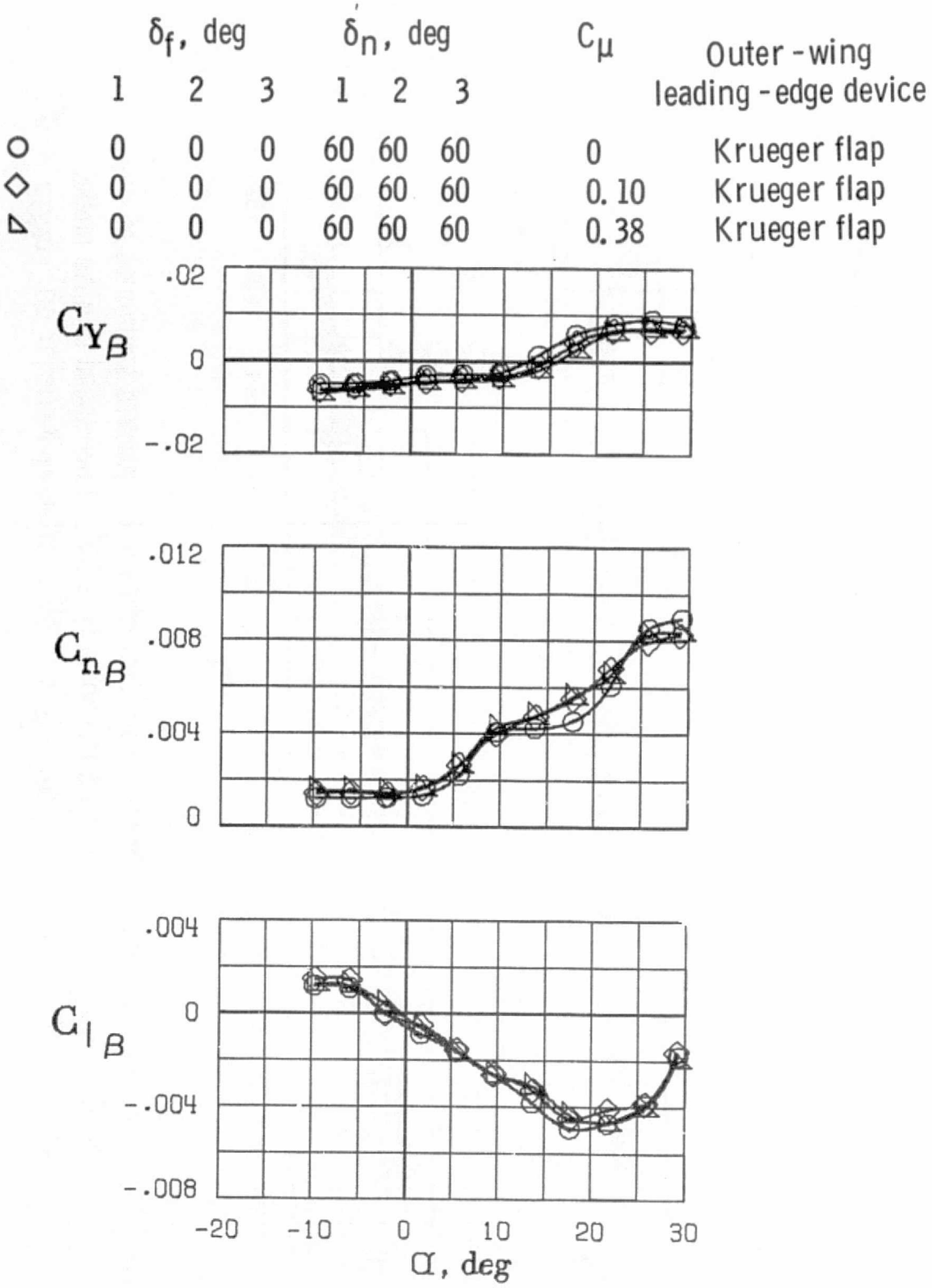

(b) Low-speed engine configuration.

Figure 20. - Concluded.

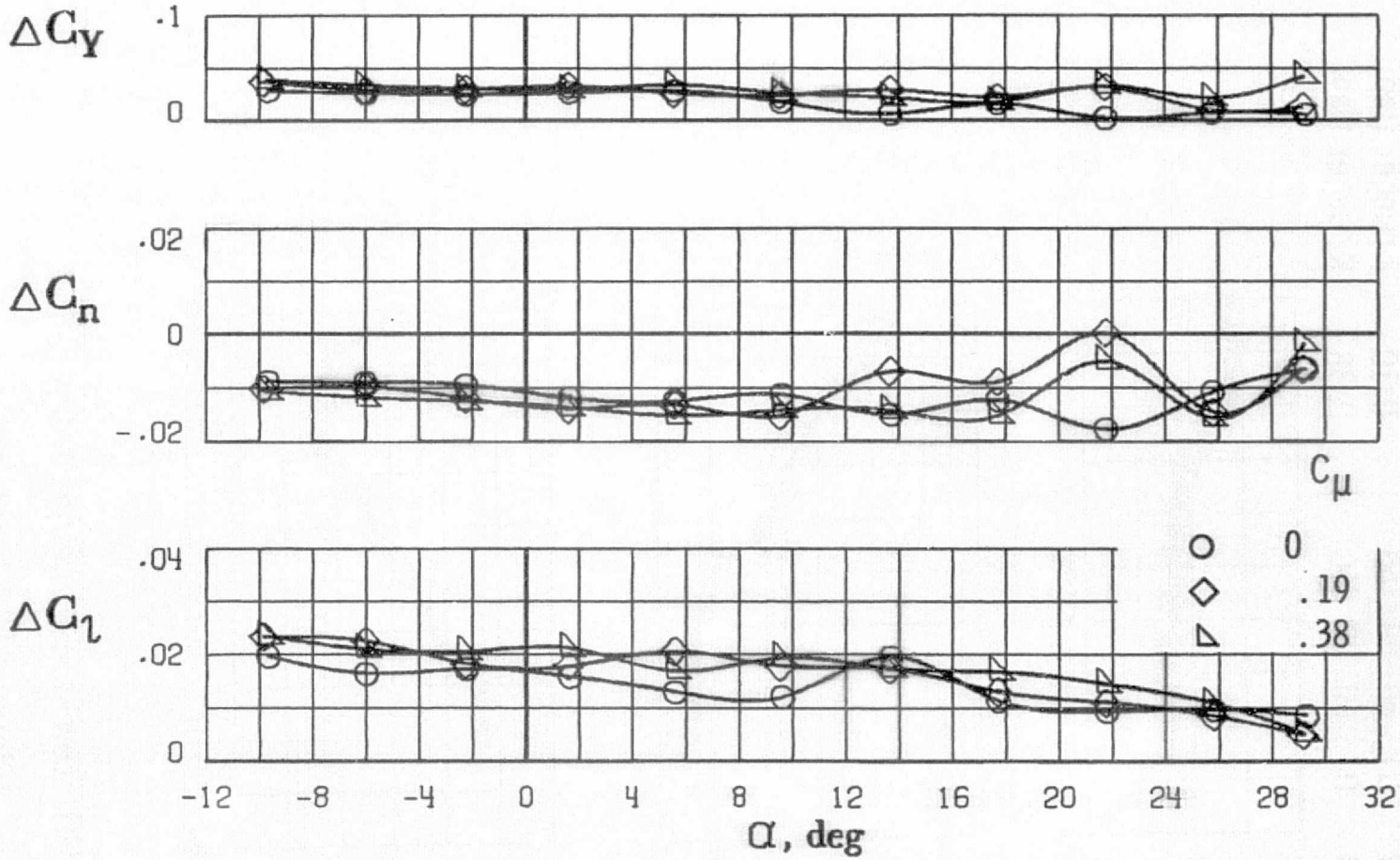

Figure 21. - Incremental lateral control characteristics with inboard segments of trailing-edge flap deflected differentially ± 30°. Low-speed engine mode. $\delta_{f,1} = 30°$, $\delta_{f,2,3} = 0°$, $\delta_{n,1,2,3} = 60°$. Wingtip Krueger on. $\delta_{NOZ} = 0°$.

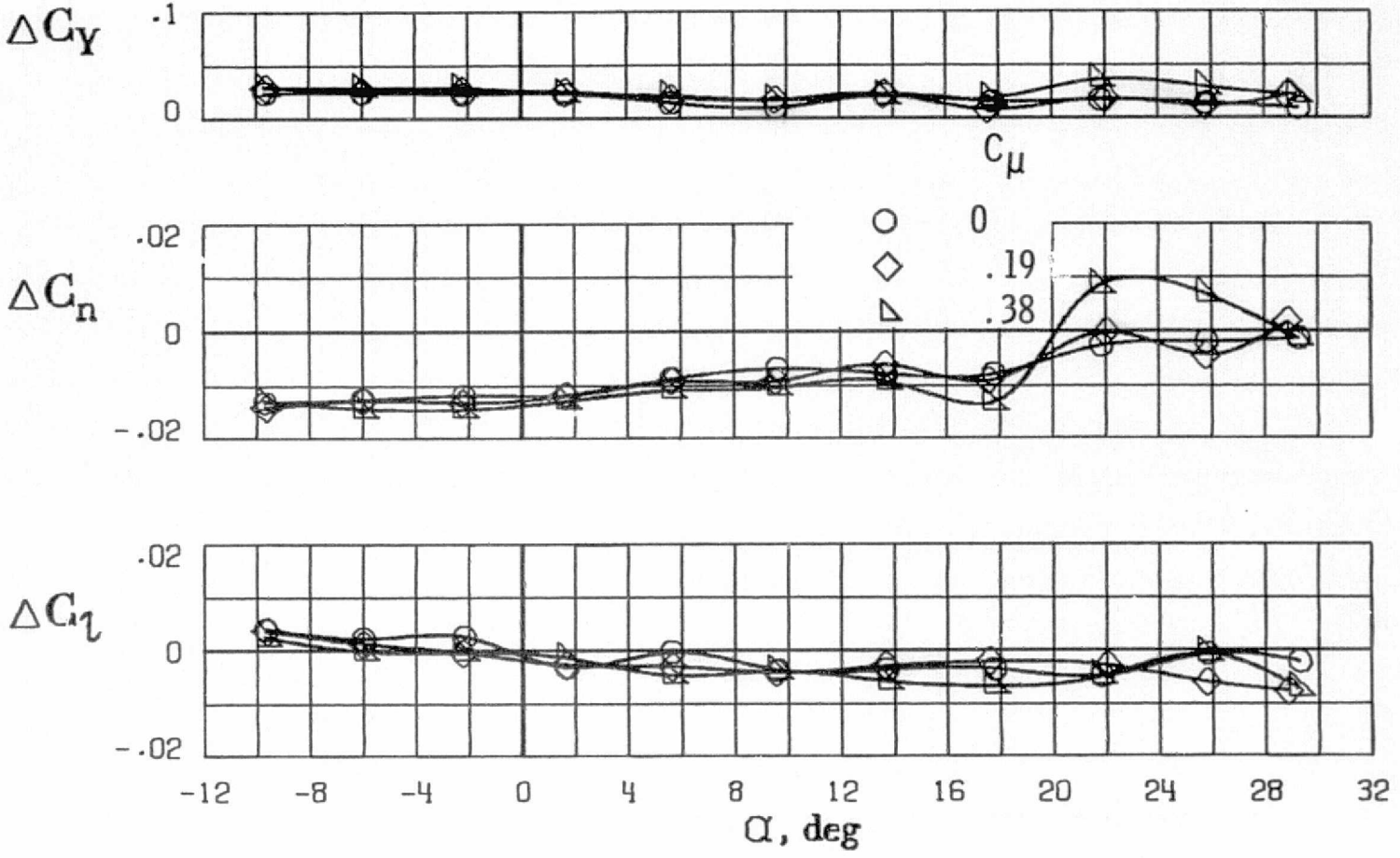

Figure 22. - Incremental lateral control characteristics with rudder deflected 30°. $\delta_{f,1,2,3} = 0°$, $\delta_{n,1,2,3} = 60°$, $\delta_r = 30°$. Low-speed engine mode. Wingtip Krueger on. $\delta_{NOZ} = 0°$.